Available online at www.sciencedirect.com

ScienceDirect

Nuclear Physics B 885 (2014) 542–570

NUCLEAR PHYSICS B

www.elsevier.com/locate/nuclphysb

The Zee–Babu model revisited in the light of new data

Juan Herrero-Garcia [a,b], Miguel Nebot [c], Nuria Rius [a,b], Arcadi Santamaria [a,b,*]

[a] *Departament de Física Teòrica, Universitat de València, Dr. Moliner 50, E-46100 Burjassot (València), Spain*
[b] *IFIC, Universitat de València-CSIC, Parque Científico, C/ Catedrático José Beltrán, 2, E-46980 Paterna, Spain*
[c] *Centro de Física Teórica de Partículas, Instituto Superior Técnico – Universidade de Lisboa, Av. Rovisco Pais 1, 1049-001 Lisboa, Portugal*

Received 26 February 2014; received in revised form 22 May 2014; accepted 4 June 2014

Available online 10 June 2014

Editor: Tommy Ohlsson

Abstract

We update previous analyses of the Zee–Babu model in the light of new data, e.g., the mixing angle θ_{13}, the rare decay $\mu \to e\gamma$ and the LHC results. We also analyze the possibility of accommodating the deviations in $\Gamma(H \to \gamma\gamma)$ hinted by the LHC experiments, and the stability of the scalar potential. We find that neutrino oscillation data and low energy constraints are still compatible with masses of the extra charged scalars accessible to LHC. Moreover, if any of them is discovered, the model can be falsified by combining the information on the singly and doubly charged scalar decay modes with neutrino data. Conversely, if the neutrino spectrum is found to be inverted and the CP phase δ is quite different from π, the masses of the charged scalars will be well outside the LHC reach.

1. Introduction

The observed pattern of neutrino masses and mixing remains one of the major puzzles in particle physics. Moreover, massive neutrinos provide irrefutable evidence for physics beyond the Standard Model (SM) and many theoretical possibilities have been proposed to account for the lightness of neutrinos (see [1–4] for some reviews). With the running of the LHC, it is timely to

* Corresponding author.

http://dx.doi.org/10.1016/j.nuclphysb.2014.06.001

explore neutrino mass models in which the scale of new physics is close to the TeV. In particular, radiative mechanisms are especially appealing, since small neutrino masses are generated naturally due to loop factors. On the other hand, new physics effects can be sizable also in low energy experiments, for instance lepton flavor violating rare decays of charged leptons, $\ell_\alpha \to \ell_\beta \gamma$, providing complementary probes for such models.

In this paper we consider the Zee–Babu model (ZB) of neutrino masses,[1] which just adds two (singly and doubly) charged scalar singlets to the SM. Neutrino masses are generated at two loops and are proportional to the Yukawa couplings of the new scalars and inversely proportional to the square of their masses. This is phenomenologically quite interesting because the new scalars cannot be very heavy or have very small Yukawa couplings, otherwise neutrino masses would be too small. As a consequence, such scalars may be accessible at the LHC, and in principle they could explain the slight excess over the SM prediction found by ATLAS in the diphoton Higgs decay channel $H \to \gamma\gamma$ (currently CMS does not see any excess, see Section 3 for the latest data). They also mediate a variety of lepton flavor violating (LFV) processes, leading to rates measurable in current experiments.

The phenomenology of the ZB model has been widely analyzed: neutrino oscillation data was used to constrain the parameter space of the model, LFV charged lepton decay rates calculated and collider signals discussed [10–12]. Non-standard neutrino interactions in the ZB model have also been thoroughly studied, in correlation with possible LHC signals and LFV processes [13]. In [12], some of us performed an exhaustive numerical study of the full parameter space of the model using Monte Carlo Markov Chain (MCMC) techniques, which allow to efficiently explore high-dimensional spaces. However, in the last few years there have been several experimental results which motivate an up-to-date analysis including all relevant data currently available. Therefore, in this work we update previous analysis in the light of the recent measurement of the neutrino mixing angle θ_{13} [14–16], the new MEG limits on $\mu \to e\gamma$ [17], the lower bounds on doubly-charged scalars coming from LHC data [18,19], and, of course, the discovery of a 125 GeV Higgs boson by ATLAS and CMS [20,21]. Moreover, we also study the possibility of accommodating deviations from the SM prediction for the Higgs diphoton decay channel, and the effects of the new couplings of the model in the stability of the scalar potential. A possible enhancement of the Higgs diphoton decay rate in the ZB model together with the vacuum stability of the scalar potential has been studied in [22], however a consistent updated analysis including all constraints is lacking.

The outline of the paper is the following. In Section 2 we briefly review the main features of the ZB model, discussing perturbativity and naturality estimates for the allowed ranges of the free parameters of the model. We summarize present constraints from recent neutrino oscillation data, low energy lepton-flavor violating processes, universality and stability of the scalar potential. We also review the collider phenomenology of the ZB model, discussing current limits from LHC, and briefly comment on the prospects for non-standard neutrino interactions. In Section 3 we analyze in detail the contributions of the ZB charged scalars to both, $\Gamma(H \to \gamma\gamma)$ and $\Gamma(H \to Z\gamma)$. After some analytic estimates in Section 4, we present the results of our MCMC numerical analysis in Section 5 and we conclude in Section 6. Renormalization group equations for the ZB model and relevant loop functions are collected in Appendices A and B.

[1] The model was first proposed in [5] and studied carefully in [6]. Similar models with a doubly charged scalar and masses generated at two loops were discussed in [7] (two-loop neutrino mass models containing doubly-charged singlets have also been recently discussed in connection with neutrinoless double beta decay [8,9]).

2. The Zee–Babu model

We follow the notation of [12]. As mentioned above, the Zee–Babu model only contains, in addition to the SM, two charged singlet scalar fields

$$h^{\pm}, \qquad k^{\pm\pm}, \tag{1}$$

with weak hypercharges ± 1 and ± 2 respectively (we use the convention $Q = T_3 + Y$).

The scalar potential is given by

$$\begin{aligned} V = {} & m_H'^2 H^\dagger H + m_h'^2 |h|^2 + m_k'^2 |k|^2 + \lambda_H \left(H^\dagger H\right)^2 + \lambda_h |h|^4 + \lambda_k |k|^4 \\ & + \lambda_{hk} |h|^2 |k|^2 + \lambda_{hH} |h|^2 H^\dagger H + \lambda_{kH} |k|^2 H^\dagger H + \left(\mu h^2 k^{++} + \text{h.c.}\right), \end{aligned} \tag{2}$$

being H the $SU(2)$ doublet Higgs boson, while the leptons have Yukawa couplings to both H and the new charged scalars:

$$\mathcal{L}_Y = \overline{L_L} Y e H + \overline{\tilde{L}_L} f \ell h^+ + \overline{e^c} g e k^{++} + \text{h.c.}, \tag{3}$$

where L_L and e are the SM $SU(2)$ lepton doublets and singlets, respectively, and $\tilde{L}_L \equiv i\tau_2 L_L^c = i\tau_2 C \overline{L_L}^T$, with τ_2 Pauli's second matrix. Due to Fermi statistics, f_{ab} is an antisymmetric matrix in flavor space while g_{ab} is symmetric.

Notice that we can assign lepton number -2 to both scalars, h^+ and k^{++}, in such a way that total lepton number L (or $B - L$) is conserved in the complete Lagrangian, except for the trilinear coupling μ of the scalar potential; thus, lepton number is explicitly broken by the μ-coupling. It is important to remark that lepton number violation requires the simultaneous presence of the four couplings Y, f, g and μ, because if any of them vanishes one can always assign quantum numbers in such a way that there is a global $U(1)$ symmetry. This means that neutrino masses will require the simultaneous presence of the four couplings.

Regarding the physical free parameters in the ZB model, our convention is the following: without loss of generality, we choose the 3×3 charged lepton Yukawa matrix Y to be diagonal with real and positive elements. We also use fermion field rephasings to remove three phases from the elements of the matrix g and charged scalar rephasings to set μ real and positive, and to remove one phase from f. In summary we have 12 moduli (3 from Y, 3 from f and 6 from g_{ab}), 5 phases (3 from g and 2 from f) and the real and positive parameter μ, plus the rest of real parameters in the scalar potential. As discussed in [12], this choice is compatible with the standard parametrization of neutrino masses and mixings.

After electroweak symmetry breaking, the masses of charged leptons are $m_a = Y_{aa} v$, with $v \equiv \langle H^0 \rangle = 174$ GeV, the VEV of the standard Higgs doublet, while the physical charged scalar masses are given by

$$m_h^2 = m_h'^2 + \lambda_{hH} v^2, \qquad m_k^2 = m_k'^2 + \lambda_{kH} v^2. \tag{4}$$

In principle, the scale of the new mass parameters of the ZB model (m_h, m_k and μ) is arbitrary. However from the experimental point of view it is interesting to consider new scalars light enough to be produced in the second run of the LHC. Also theoretical arguments suggest that the scalar masses should be relatively light (few TeV), to avoid unnaturally large one-loop corrections to the Higgs mass which would introduce a hierarchy problem. Therefore, in this paper we will focus on the masses of the new scalars, m_h, m_k, below 2 TeV.

The Yukawa couplings of the new scalars of the model enter in the neutrino mass formula and in several LFV processes, and are strongly bounded for the scalar masses we are considering except in a few corners of the parameter space where we require that the theory remains perturbative. Since one-loop corrections to Yukawa couplings are order

$$\delta f \sim \frac{f^3}{(4\pi)^2}, \qquad \delta g \sim \frac{g^3}{(4\pi)^2} \tag{5}$$

one expects from perturbativity $f, g \ll 4\pi$, although, as we will see, for the scalar masses considered here, phenomenological constraints are always stronger.

The couplings of the charged scalars in the scalar potential, apart from the stability constraints described in Section 2.5, are essentially free. However, for the theory to make sense as a perturbative theory we also impose the limit[2] $\lambda_{h,k,kH,hH,hk} < 4\pi$.

The trilinear coupling among charged scalars μ, on the other hand, is different, for it has dimensions of mass and it is insensitive to high energy perturbative unitarity constraints. However, it induces radiative corrections to the masses of the charged scalars of order

$$\delta m_k^2, \delta m_h^2 \sim \frac{\mu^2}{(4\pi)^2}. \tag{6}$$

Requiring that the corrections in absolute value are much smaller than the masses we can derive a naive upper bound for this parameter, $\mu \ll 4\pi \min(m_h, m_k)$, but it is difficult to fix an exact value of μ for which the contributions to the scalar masses are unacceptably large, leading to a highly fine-tuned scenario.

A large value of μ, as compared with scalar masses, is also disfavored because it could lead to a deeper minimum of the scalar potential for non-vanishing values of the charged fields, therefore breaking charge conservation. This phenomenon has also been studied in the context of supersymmetric theories (see for instance [25–27]). As an example, by looking at the particular direction $|H| = |h| = |k| = r$, and requiring that the charge breaking minimum is not a global minimum, $V(r \neq 0) > 0$, one obtains

$$\mu^2 < (\lambda_H + \lambda_h + \lambda_k + \lambda_{hH} + \lambda_{kH} + \lambda_{hk})\left(m_H'^2 + m_h'^2 + m_k'^2\right). \tag{7}$$

Assuming no cancellations between the λ's or mass terms, neglecting λ_H and $m_H'^2$, and using the perturbative limit for the rest of the couplings $\lambda_i \lesssim 4\pi$ one finds a very conservative bound on μ

$$\mu \lesssim \sqrt{20\pi} \max(m_k, m_h) \sim 8 \max(m_k, m_h). \tag{8}$$

Tighter limits can be obtained by looking at all directions in the potential and/or allowing for cancellations.

Given that the neutrino masses depend linearly on the parameter μ, as we will see in the next section, the ability of the model to accommodate all present data is quite sensitive to the upper limit allowed for μ. Thus we choose to implement such limit in terms of a parameter κ,

$$\mu < \kappa \min(m_h, m_k), \tag{9}$$

[2] Notice that there could be order one differences in the perturbativity constraints on the different couplings λ_i from perturbative unitarity of the matrix elements [23,24]. We can neglect them for the purpose of this work, keeping in mind that they could be relevant when perturbativity is "pushed" to the limit (as needed to explain $H \to \gamma\gamma$ enhancement, see Section 3).

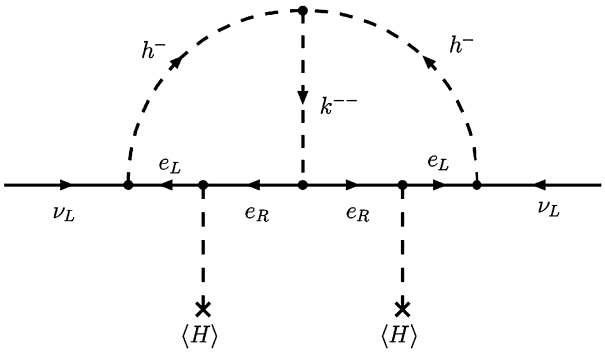

Fig. 1. Diagram contributing to the neutrino Majorana mass at two loops.

and discuss our results for different values of $\kappa = 1, 5, 4\pi$. Notice that we are using the naturality upper bound (expressed in terms of $\min(m_h, m_k)$), which in general is much more restrictive than the upper bound obtained by requiring that the minimum of the potential does not break charge conservation (expressed in terms of $\max(m_h, m_k)$).

2.1. Neutrino masses

The lowest order contribution to neutrino masses involving the four relevant couplings appears at two loops [5,6] and its Feynman diagram is depicted in Fig. 1.

The calculation of this diagram gives the following mass matrix for the neutrinos (defined as an effective term in the Lagrangian $\mathcal{L}_\nu \equiv -\frac{1}{2}\overline{\nu_L^c}\mathcal{M}_\nu \nu_L + \text{h.c.}$)

$$(\mathcal{M}_\nu)_{ij} = 16\mu f_{ia} m_a g^*_{ab} I_{ab} m_b f_{jb}, \tag{10}$$

where I_{ab} is the two-loop integral, which can be calculated analytically [28]. However, since m_c, m_d are the masses of the charged leptons, necessarily much lighter than the charged scalars, we can neglect them and obtain a much simpler form

$$I_{cd} \simeq I = \frac{1}{(16\pi^2)^2}\frac{1}{M^2}\frac{\pi^2}{3}\tilde{I}(r), \quad M \equiv \max(m_h, m_k), \tag{11}$$

where $\tilde{I}(r)$ is a function of the ratio of the masses of the scalars $r \equiv m_k^2/m_h^2$,

$$\tilde{I}(r) = \begin{cases} 1 + \frac{3}{\pi^2}(\log^2 r - 1) & \text{for } r \gg 1 \\ 1 & \text{for } r \to 0, \end{cases} \tag{12}$$

which is close to one for a wide range of scalar masses. Within this approximation the neutrino mass matrix can be directly written in terms of the Yukawa coupling matrices, f, g, and Y

$$\mathcal{M}_\nu = \frac{v^2\mu}{48\pi^2 M^2}\tilde{I} f Y g^\dagger Y^T f^T. \tag{13}$$

A very important point is that since f is a 3×3 antisymmetric matrix, $\det f = 0$ (for 3 generations), and therefore $\det \mathcal{M}_\nu = 0$. Thus, at least one of the neutrinos is exactly massless at this order.

The neutrino Majorana mass matrix $\mathcal{M}_\nu$ can be written as

$$\mathcal{M}_\nu = U D_\nu U^T, \tag{14}$$

where D_ν is a diagonal matrix with real positive eigenvalues, and U is the Pontecorvo–Maki–Nakagawa–Sakata (PMNS) leptonic mixing matrix. We are left with only two possibilities for the neutrino masses, m_i:

- Normal hierarchy (NH): the solar squared mass difference is $\Delta_S = m_2^2$, the atmospheric mass splitting $\Delta_A = m_3^2$ and $m_1 = 0$, with $m_3 \gg m_2$.
- Inverted hierarchy (IH): $\Delta_S = m_2^2 - m_1^2$, $\Delta_A = m_1^2$ and $m_3 = 0$, with $m_1 \approx m_2$.

The standard parametrization for the PMNS matrix is

$$U = \begin{pmatrix} c_{13}c_{12} & c_{13}s_{12} & s_{13}e^{-i\delta} \\ -c_{23}s_{12} - s_{23}s_{13}c_{12}e^{i\delta} & c_{23}c_{12} - s_{23}s_{13}s_{12}e^{i\delta} & s_{23}c_{13} \\ s_{23}s_{12} - c_{23}s_{13}c_{12}e^{i\delta} & -s_{23}c_{12} - c_{23}s_{13}s_{12}e^{i\delta} & c_{23}c_{13} \end{pmatrix} \begin{pmatrix} 1 & & \\ & e^{i\phi/2} & \\ & & 1 \end{pmatrix}, \tag{15}$$

where $c_{ij} \equiv \cos\theta_{ij}$, $s_{ij} \equiv \sin\theta_{ij}$ and since one of the neutrinos is massless, there is only one physical Majorana phase, ϕ, in addition to the Dirac phase δ.

2.2. Low energy constraints

In order to provide neutrino masses compatible with experiment, the Yukawa couplings of the charged scalars cannot be too small and their masses cannot be too large. This immediately gives rise to a series of flavor lepton number violating processes, as for instance $\mu^- \to e^-\gamma$ or $\mu^- \to e^+e^-e^-$, with rates which can be, in some cases, at the verge of the present experimental limits. Therefore, we can use these processes to obtain information about the parameters of the model and hopefully to confirm or to exclude the model in a near future by exploiting the synergies with direct searches for the new scalars at LHC.

In this section we follow the notation of [12], where all the relevant formulae can be found, and update the new bounds. We collect the relevant tree-level lepton flavor violating constraints, from $\ell_a^- \to \ell_b^+\ell_c^-\ell_d^-$ decays and $\mu^+e^- \leftrightarrow \mu^-e^+$ transitions, in Table 1.

Finally, one-loop level lepton flavor violating constraints coming from $\ell_a^- \to \ell_b^-\gamma$ decays[3] and anomalous magnetic moments of electron and muon are collected in Table 3, including the recent limit on BR($\mu \to e\gamma$) from the MEG Collaboration [17].

Universality constraints are summarized in Table 2 where we have combined the measurements presented in [29] for the different couplings. There seems to be a 2σ discrepancy in $G_\tau^{\rm exp}/G_e^{\rm exp}$, which we interpret as a bound. If confirmed and interpreted within the ZB model, one obtains that $|f_{\mu\tau}|^2 - |f_{e\mu}|^2 = 0.05\ (m_h/\text{TeV})^2$. As we will see in Section 4, for NH spectrum $f_{e\mu} \sim f_{\mu\tau}/2$, therefore one needs $m_h \sim 4 f_{\mu\tau}$ TeV, which is easily achieved. For IH spectrum, however, $f_{\mu\tau} \sim 0.2 f_{e\mu}$ ($f_{\mu\tau} \sim (0.15\text{–}0.3)\ f_{e\mu}$ if we vary the angles in their 3σ range), and therefore, if this measurement is confirmed, the IH scheme in the ZB model would be disfavored.

[3] As was shown in [30], doubly charged scalars can give logarithmic enhanced contributions to muon–electron conversion in nuclei. Moreover, planned experiments will improve current limits by four orders of magnitude [31–33]; however, at present, limits are still not competitive with $\mu \to e\gamma$.

Table 1
Constraints from tree-level lepton flavor violating decays [3].

Process	Experiment (90% C.L.)	Bound (90% C.L.)
$\mu^- \to e^+e^-e^-$	$\mathrm{BR} < 1.0 \times 10^{-12}$	$\lvert g_{e\mu} g^*_{ee}\rvert < 2.3 \times 10^{-5}\ (\frac{m_k}{\mathrm{TeV}})^2$
$\tau^- \to e^+e^-e^-$	$\mathrm{BR} < 2.7 \times 10^{-8}$	$\lvert g_{e\tau} g^*_{ee}\rvert < 0.009\ (\frac{m_k}{\mathrm{TeV}})^2$
$\tau^- \to e^+e^-\mu^-$	$\mathrm{BR} < 1.8 \times 10^{-8}$	$\lvert g_{e\tau} g^*_{e\mu}\rvert < 0.005\ (\frac{m_k}{\mathrm{TeV}})^2$
$\tau^- \to e^+\mu^-\mu^-$	$\mathrm{BR} < 1.7 \times 10^{-8}$	$\lvert g_{e\tau} g^*_{\mu\mu}\rvert < 0.007\ (\frac{m_k}{\mathrm{TeV}})^2$
$\tau^- \to \mu^+e^-e^-$	$\mathrm{BR} < 1.5 \times 10^{-8}$	$\lvert g_{\mu\tau} g^*_{ee}\rvert < 0.007\ (\frac{m_k}{\mathrm{TeV}})^2$
$\tau^- \to \mu^+e^-\mu^-$	$\mathrm{BR} < 2.7 \times 10^{-8}$	$\lvert g_{\mu\tau} g^*_{e\mu}\rvert < 0.007\ (\frac{m_k}{\mathrm{TeV}})^2$
$\tau^- \to \mu^+\mu^-\mu^-$	$\mathrm{BR} < 2.1 \times 10^{-8}$	$\lvert g_{\mu\tau} g^*_{\mu\mu}\rvert < 0.008\ (\frac{m_k}{\mathrm{TeV}})^2$
$\mu^+e^- \to \mu^-e^+$	$G_{M\bar{M}} < 0.003 G_F$	$\lvert g_{ee} g^*_{\mu\mu}\rvert < 0.2\ (\frac{m_k}{\mathrm{TeV}})^2$

Table 2
Constraints from universality of charged currents obtained combining the experimental results compiled in Table 2 of [29].

SM Test	Experiment	Bound (90% C.L.)
lept./hadr. univ.	$\sum_{q=d,s,b} \lvert V^{\mathrm{exp}}_{uq}\rvert^2 = 0.9999 \pm 0.0006$	$\lvert f_{e\mu}\rvert^2 < 0.007\ (\frac{m_h}{\mathrm{TeV}})^2$
μ/e universality	$\frac{G^{\mathrm{exp}}_\mu}{G^{\mathrm{exp}}_e} = 1.0010 \pm 0.0009$	$\lvert\lvert f_{\mu\tau}\rvert^2 - \lvert f_{e\tau}\rvert^2\rvert < 0.024\ (\frac{m_h}{\mathrm{TeV}})^2$
τ/μ universality	$\frac{G^{\mathrm{exp}}_\tau}{G^{\mathrm{exp}}_\mu} = 0.9998 \pm 0.0013$	$\lvert\lvert f_{e\tau}\rvert^2 - \lvert f_{e\mu}\rvert^2\rvert < 0.035\ (\frac{m_h}{\mathrm{TeV}})^2$
τ/e universality	$\frac{G^{\mathrm{exp}}_\tau}{G^{\mathrm{exp}}_e} = 1.0034 \pm 0.0015$	$\lvert\lvert f_{\mu\tau}\rvert^2 - \lvert f_{e\mu}\rvert^2\rvert < 0.04\ (\frac{m_h}{\mathrm{TeV}})^2$

Table 3
Constraints from loop-level lepton flavor violating interactions and anomalous magnetic moments [3,17].

Experiment	Bound (90% C.L.)
$\delta a_e = (12 \pm 10) \times 10^{-12}$	$r(\lvert f_{e\mu}\rvert^2 + \lvert f_{e\tau}\rvert^2) + 4(\lvert g_{ee}\rvert^2 + \lvert g_{e\mu}\rvert^2 + \lvert g_{e\tau}\rvert^2) < 5.5 \times 10^3\ (m_k/\mathrm{TeV})^2$
$\delta a_\mu = (21 \pm 10) \times 10^{-10}$	$r(\lvert f_{e\mu}\rvert^2 + \lvert f_{\mu\tau}\rvert^2) + 4(\lvert g_{e\mu}\rvert^2 + \lvert g_{\mu\mu}\rvert^2 + \lvert g_{\mu\tau}\rvert^2) < 7.9\ (m_k/\mathrm{TeV})^2$
$\mathrm{BR}(\mu \to e\gamma) < 5.7 \times 10^{-13}$	$r^2\lvert f^*_{e\tau} f_{\mu\tau}\rvert^2 + 16\lvert g^*_{ee} g_{e\mu} + g^*_{e\mu} g_{\mu\mu} + g^*_{e\tau} g_{\mu\tau}\rvert^2 < 1.6 \times 10^{-6}\ (m_k/\mathrm{TeV})^4$
$\mathrm{BR}(\tau \to e\gamma) < 3.3 \times 10^{-8}$	$r^2\lvert f^*_{e\mu} f_{\mu\tau}\rvert^2 + 16\lvert g^*_{ee} g_{e\tau} + g^*_{e\mu} g_{\mu\tau} + g^*_{e\tau} g_{\tau\tau}\rvert^2 < 0.52\ (m_k/\mathrm{TeV})^4$
$\mathrm{BR}(\tau \to \mu\gamma) < 4.4 \times 10^{-8}$	$r^2\lvert f^*_{e\mu} f_{e\tau}\rvert^2 + 16\lvert g^*_{e\mu} g_{e\tau} + g^*_{\mu\mu} g_{\mu\tau} + g^*_{\mu\tau} g_{\tau\tau}\rvert^2 < 0.7\ (m_k/\mathrm{TeV})^4$

Given that lepton number is not conserved, another interesting low energy process that could arise in the ZB model is neutrinoless double beta decay ($0\nu2\beta$). However, since the singly and doubly charged scalars do not couple to hadrons and are singlet under the weak $SU(2)$ (therefore, do not couple to W gauge bosons), the $0\nu2\beta$ rate is dominated by the Majorana neutrino exchange [34] and it is proportional to the $\lvert(\mathcal{M}_\nu)_{ee}\rvert^2$ matrix element. In the NH case,

$$\left(\mathcal{M}^{NH}_\nu\right)_{ee} = \sqrt{\Delta_S} c^2_{13} s^2_{12} e^{i\phi} + \sqrt{\Delta_A} s^2_{13}. \tag{16}$$

Using neutrino oscillation data, one obtains $0.001 \lesssim \mathrm{eV}\lvert(\mathcal{M}^{NH}_\nu)_{ee}\rvert \lesssim 0.004$ eV and therefore it is outside the reach of present and near future $0\nu2\beta$ decay experiments.

In the IH case,

$$\left(\mathcal{M}^{IH}_\nu\right)_{ee} = \sqrt{\Delta_A + \Delta_S} c^2_{13} s^2_{12} e^{i\phi} + \sqrt{\Delta_A} c^2_{13} c^2_{12}. \tag{17}$$

Then, 0.01 eV $\lesssim |(\mathcal{M}_\nu^{NH})_{ee}| \lesssim$ 0.05 eV and, therefore, it is observable in planned $0\nu2\beta$ decay experiments.

2.3. Non-standard interactions

The heavy scalars of the ZB model induce non-standard lepton interactions at tree level, which have been thoroughly analyzed in [13]. In particular, by integrating out the singly charged scalar h^+, the following dimension-6 operators are generated:

$$\mathcal{L}_{d=6}^{NSI} = 2\sqrt{2}G_F\epsilon_{\alpha\beta}^{\rho\sigma}\left(\overline{\nu_\alpha}\gamma^\mu P_L\nu_\beta\right)(\overline{\ell_\rho}\gamma_\mu P_L\ell_\sigma), \tag{18}$$

where ℓ refer to the charged leptons and the standard NSI parameters $\epsilon_{\alpha\beta}^{\rho\sigma}$ are given by

$$\epsilon_{\alpha\beta}^{\rho\sigma} = \frac{f_{\sigma\beta}f_{\rho\alpha}^*}{\sqrt{2}G_F m_h^2}. \tag{19}$$

Regarding neutrino propagation in matter, the relevant NSI parameters are $\epsilon_{\alpha\beta}^m = \epsilon_{\alpha\beta}^{ee}$. Since the couplings $f_{\sigma\beta}$ are antisymmetric, in the ZB model only $\epsilon_{\mu\tau}^m$, $\epsilon_{\mu\mu}^m$ and $\epsilon_{\tau\tau}^m$ are non-zero.

NSI can also affect the neutrino production in a neutrino factory, via the processes $\mu \to e\overline{\nu_\beta}\nu_\alpha$. Source effects in the $\nu_\mu \to \nu_\tau$ and $\nu_e \to \nu_\tau$ channels are produced by the NSI parameters

$$\epsilon_{\mu\tau}^s = \epsilon_{\tau e}^{e\mu} = \frac{f_{\mu e}f_{e\tau}^*}{\sqrt{2}G_F m_h^2}, \tag{20}$$

$$\epsilon_{e\tau}^s = \epsilon_{\mu\tau}^{e\mu} = \frac{f_{\mu\tau}f_{e\mu}^*}{\sqrt{2}G_F m_h^2}, \tag{21}$$

respectively. Notice that $\epsilon_{\mu\tau}^m = -\epsilon_{\mu\tau}^{s*}$, since both NSI parameters are related to the couplings $f_{e\mu}$ and $f_{e\tau}$.

As we discuss in Section 5, the ratios of Yukawa couplings $f_{e\mu}/f_{\mu\tau}$ and $f_{e\tau}/f_{\mu\tau}$ are entirely determined by the neutrino mixing angles and Dirac phase of the PMNS matrix U – see Eqs. (37) and (38) –, so the impact of the improved bounds on BR($\mu \to e\gamma$) can be easily estimated: given that the limit is now ∼0.05 times smaller than in the study of [13], and the contribution of the singly charged scalar h^+ to BR($\mu \to e\gamma$) depends on $|f_{e\tau}^* f_{\mu\tau}|^2$, the current constraints on $|f_{\alpha\beta}|$ are roughly a factor 2 tighter than before. Therefore, since the strength of the NSI depends on $\epsilon_{\alpha\beta}^{\rho\sigma} \propto f_{\sigma\beta}f_{\rho\alpha}^*$, generically we expect that the allowed size of the NSI is reduced by a factor ∼1/4. According to [13],[4] this implies that in the most favorable case of IH neutrino mass spectrum, $\epsilon_{e\tau}^s$ and $\epsilon_{\mu\tau}^s$ are in the range $3 \times (10^{-5}$–$10^{-4})$, which is in a range difficult to probe, but it might be in a future neutrino factory with a ν_τ near detector [35].

2.4. Bounds on the masses of the charged scalars

Regarding limits on singly-charged bosons decaying to leptons, the best limit still comes from LEP II, $m_h > 100$ GeV.

[4] Notice that although the analysis of [13] has been done for $\kappa = 1$, the impact on NSI of the new bounds from BR($\mu \to e\gamma$) (and in general from any LFV decay $\ell_\alpha \to \ell_\beta\gamma$) is independent of the value of κ chosen, because they constraint directly $|f_{\alpha\sigma}^* f_{\sigma\beta}|/m_h^2$, which is the same combination that appears in the NSI parameters, Eq. (19). The only effect of increasing κ may be that a given point $(f_{\alpha\sigma}, f_{\sigma\beta}, m_h)$ is able to fit neutrino masses with smaller g_{ab} and therefore possibly lighter m_k.

ATLAS and CMS have placed limits on doubly-charged boson masses from searches of dilepton final states, using data samples corresponding to $\sqrt{s} = 7$ TeV with an integrated luminosity of 4.7 fb^{-1} and 4.9 fb^{-1}, respectively [18,19]. The authors of [36] show that, with current data at 8 TeV and 20 fb^{-1}, all the bounds are expected to become about ∼100 GeV more stringent if no significant signal is seen. Further tests on the nature of the doubly charged scalar (i.e., singlet or triplet of $SU(2)_L$) can be obtained by analyzing tau lepton decay distributions which are sensitive to the chiral structure of the couplings [37]. The main production mechanisms of doubly-charged bosons at hadron colliders are pair production via an s-channel exchange of a photon or a Z-boson, and associated production with a charged boson via the exchange of a W-boson (see [38,39] for a general analysis of the production and detection at LHC of doubly charged scalars belonging to different electroweak representations). In the Zee–Babu model, the associated production is absent, because the new scalars are $SU(2)_L$ singlets.

The ATLAS analysis [18] focuses on the $ee, \mu\mu, e\mu$ channels and assumes that the rest of the channels can make up to 90% of the total decays. Then, the limits for the Zee–Babu model are, at the 95% C.L., 322, 306, 310 GeV (151, 176, 151 GeV) for branching ratios of 100% (10%) to the $ee, \mu\mu, e\mu$ channels. Notice that in [18] the limits on doubly-charged bosons coupling to left-handed leptons are applied, in addition to the seesaw type II case, to the Zee–Babu model. However, this is not so, as the doubly-charged singlets in the Zee–Babu model are $SU(2)_L$ singlets and thus couple only to right-handed leptons, at variance with the seesaw type II models, where the doubly-charged bosons are $SU(2)_L$ triplets and do couple only to left-handed leptons. Therefore, in the Zee–Babu case they have a reduced production cross section, due to their different couplings to the Z-boson, around 2.5 times smaller than for the case of the triplet [40], and less stringent limits apply: for the Zee–Babu model one should look at the second part of Table I of [18], the one for $H_R^{\pm\pm} \equiv k^{\pm\pm}$.

The CMS Collaboration has searched for doubly-charged bosons which are $SU(2)_L$ triplets, both assuming that they decay to the different dilepton final states $\ell\ell$ ($\ell = e, \mu, \tau$) 100% of the times, i.e., BR($k^{++} \to \ell\ell$) = 1, and also considering several benchmark points with different branching ratios.

The CMS 95% C.L. limits for pair production of $SU(2)_L$ singlets, which is the one relevant for the Zee–Babu model, are around 60–80 GeV less stringent [39,40]:

- $ee, \mu\mu, e\mu$: 310 GeV,
- $e\tau, \mu\tau$: 220 GeV,
- $\tau\tau$: 100 GeV.

Note that whenever the branching ratio to $\tau\tau$ is less than 30% (see Tables I and VI of [19]), the bounds are ∼280 GeV, provided that there is a significant fraction of decays into light leptons ($ee, \mu\mu, e\mu$).

In the Zee–Babu model the decay width of $k^{\pm\pm}$ into same sign leptons is given by

$$\Gamma(k \to \ell_a \ell_b) = \frac{|g_{ab}|^2}{4\pi(1+\delta_{ab})} m_k. \tag{22}$$

Since the g_{ab} couplings are free parameters, the BRs of the different decay modes are a priori unknown, so we cannot apply directly these bounds. As we will see in the numerical analysis, Section 5, once neutrino oscillation data and low energy constraints are taken into account, the branching ratio to $\tau\tau$ is very small in the Zee–Babu model, less than about 1%. Then, a conservative limit is $m_k > 220$ GeV.

Moreover, in the ZB model for $m_k > 2\,m_h > 200$ GeV, it can happen that the doubly charged scalar decays predominantly into hh, which can easily escape detection. This way the constraints from dilepton searches could be evaded. The relevant decay width is given by

$$\Gamma(k \to hh) = \frac{1}{8\pi}\left[\frac{\mu}{m_k}\right]^2 m_k \sqrt{1 - \frac{4m_h^2}{m_k^2}}. \tag{23}$$

Then, even for $g_{ab} \sim 1$, for $m_h = 100$ GeV and $m_k = 200$ GeV, we have that $\frac{\Gamma(k\to hh)}{\Gamma(k\to \ell\ell)} \geq 1$ for $\mu \geq m_k$, which is still natural as long it is not very large. Thus, we take $m_k \geq 200$ GeV in the numerical analysis.

2.5. *Stability of the potential*

In this section we consider further constraints on the ZB model parameter space coming from vacuum stability conditions. The Hamiltonian in quantum mechanics has to be bounded from below, this requires that the quartic part of the scalar potential in Eq. (2) should be positive for all values of the fields and for all scales. Then, if two of the fields H, k or h vanish one immediately finds[5]:

$$\lambda_H > 0, \qquad \lambda_h > 0, \qquad \lambda_k > 0. \tag{24}$$

Moreover the positivity of the potential whenever one of the scalar fields H, h, k is zero implies

$$\alpha, \beta, \gamma > -1, \tag{25}$$

where we have defined

$$\alpha = \lambda_{hH}/(2\sqrt{\lambda_H \lambda_h}), \qquad \beta = \lambda_{kH}/(2\sqrt{\lambda_H \lambda_k}), \qquad \gamma = \lambda_{hk}/(2\sqrt{\lambda_h \lambda_k}). \tag{26}$$

Eq. (25) constrains only negative mixed couplings, $\lambda_{xH}, \lambda_{hk}$ $(x = h, k)$, since for positive ones the potential is definite positive and only the perturbativity limit, $\lambda_{xH}, \lambda_{hk} \lesssim 4\pi$ applies. Finally, if at least two of the mixed couplings are negative, there is an extra constraint, which can be written as:

$$1 - \alpha^2 - \beta^2 - \gamma^2 + 2\alpha\beta\gamma > 0 \vee \alpha + \beta + \gamma > -1. \tag{27}$$

We have checked that the above conditions, Eqs. (24), (25), (27), are equivalent to the ones derived in [41] for the Zee model, but they differ from the ones used in [22] for the ZB model, which seem not to be symmetric under the exchange of α, β, γ, as they should. Our constraints also agree with the results obtained by using copositive criteria (see for instance [42]).

The discovery of the Higgs boson with mass $m_H \sim 125$ GeV at the LHC has raised the interest on the vacuum stability of the SM potential: for the current central values of the strong coupling constant and the Higgs and top quark masses, the Higgs self-coupling λ_H would turn negative at a scale $\Lambda \sim 10^{10}$–10^{13} GeV [43], indicating the existence of new physics beyond the SM below that scale. In fact, by using state of the art radiative corrections, the authors of [43] find that absolute stability of the SM Higgs potential up to the Planck scale is excluded at 98% C.L. for $m_H < 126$ GeV.

[5] We do not consider the possibility of zero couplings, which can only appear at very specific scales.

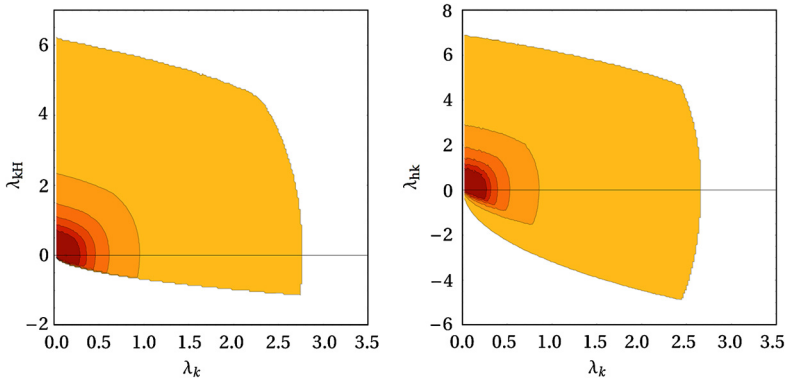

Fig. 2. Allowed regions in λ_{kH} vs λ_k (left) and λ_{hk} vs λ_h (right), taken at the m_Z scale, if perturbativity/stability is required to be valid up to 10^3, 10^6, 10^9, 10^{12}, 10^{15}, 10^{18} GeV (from light to dark colors). The rest of the parameters entering the RGE are taken at their measured value or varied in the range allowed by the perturbativity/stability requirement up to the given scale.

The one-loop renormalization group equations (RGEs) in the ZB model are written in Appendix A. For a given set of parameters defined at the electroweak scale, and satisfying the stability conditions discussed above, we calculate the running couplings numerically by using one-loop RGEs. From Eqs. (A.1), we see that the new scalar couplings $\lambda_{hH}, \lambda_{kH}$ always contribute positively to the running of the Higgs quartic coupling λ_H, compensating for the large and negative contribution of the top quark Yukawa coupling. Therefore, the vacuum stability problem can be alleviated in the ZB model with λ_H remaining positive up to the Planck scale for the present central values of m_t and m_H if λ_{xH} are not extremely small ($\lambda_{xH} \sim \pm 0.2$ are enough to stabilize λ_H maintaining stability/perturbativity of all couplings up to the Planck scale; see Fig. 2).

On the other hand, as we discuss in Section 3, the slight excess in the Higgs diphoton decay channel found at LHC can be accommodated in the ZB model with relatively light singlet scalars and large, negative, mixed couplings $\lambda_{hH}, \lambda_{kH}$. However for such values of the scalar couplings at the electroweak scale, the RGEs lead to vacuum instability ($2\sqrt{\lambda_H \lambda_x} + \lambda_{xH} < 0,\ x = h, k$) and/or non-perturbativity ($\lambda_x > 4\pi$) well below the Planck scale. This can be seen in Fig. 2 where we have performed a complete scan of the quartic couplings of the scalar potential, run all of them from m_Z up to a given scale ($\mu = 10^{3n}$ GeV with $n = 1, 2, \cdots, 6$), and check that stability (as explained before) and perturbativity ($\lambda_i < 4\pi$) are satisfied at all scales below μ. On the left we represent the region allowed in the λ_{kH}–λ_k plane, with λ's taken at the m_Z scale, when stability/perturbativity is imposed up to the different scales μ. Lighter regions correspond to small scales and obviously include the regions of larger scales. A similar plot is obtained for λ_{hH} vs λ_h. On the right we present the equivalent results for the couplings λ_{hk} vs λ_h.

3. $H \to \gamma\gamma$ and $H \to Z\gamma$

It remains an open question whether the 125 GeV Higgs boson discovered by ATLAS [20] and CMS [21] is the SM one or has some extra features coming from new physics. While all the present measurements of the Higgs properties are consistent with the SM values, the uncertainties are still large, so there is plenty of room for non-standard signals to show up in the upcoming 13–14 TeV run data. Moreover, the present experimental situation of the $H \to \gamma\gamma$ decay channel

is far from clear: although the last reported analysis of the CMS and ATLAS Collaborations on the diphoton signal strength are barely consistent with each other within 2σ, ATLAS still observes a $\sim 2\sigma$ excess over the SM prediction [44], while the CMS measurement has become consistent with the SM at 1σ [45]:

$$\begin{aligned} \text{ATLAS:} \quad & R_{\gamma\gamma} = 1.55^{+0.33}_{-0.28}, \\ \text{CMS:} \quad & R_{\gamma\gamma} = 0.78^{+0.28}_{-0.26}, \quad \text{MVA analysis} \\ \text{CMS:} \quad & R_{\gamma\gamma} = 1.11^{+0.32}_{-0.31}, \quad \text{cut based analysis.} \end{aligned} \tag{28}$$

It is thus worthwhile to explore whether an eventually confirmed deviation from the SM prediction in the $H \to \gamma\gamma$ channel can be accommodated within the ZB model.

In the SM the $H \to \gamma\gamma$ channel is dominated by the W boson loop contribution, which interferes destructively with the top quark one. Since the Higgs coupling to photons is induced at the loop-level, extra charged fermions or scalars with significant couplings to the Higgs can change drastically the $H \to \gamma\gamma$ channel with respect to the Standard Model expectations, either enhancing it or reducing it [46]. Moreover, in the absence of direct signatures of new particles at LHC, the enhanced Higgs diphoton decay rate might provide an indirect hint of physics beyond the SM.

The value of the $H \to \gamma\gamma$ decay width in the ZB model with respect to the SM one is given by [46–48]:

$$R_{\gamma\gamma} = \frac{\Gamma(H \to \gamma\gamma)_{ZB}}{\Gamma(H \to \gamma\gamma)_{SM}} = \left|1 + \delta R(m_h, \lambda_{hH}) + 4\,\delta R(m_k, \lambda_{kH})\right|^2, \tag{29}$$

where we have defined $\delta R(m_x, \lambda_{xH})$ for the scalar x with mass m_x and coupling to the Higgs λ_{xH} as:

$$\delta R(m_x, \lambda_{xH}) \equiv \frac{\lambda_{xH}\, v^2}{2m_x^2} \frac{A_0(\tau_x)}{A_1(\tau_W) + \frac{4}{3}A_{1/2}(\tau_t)}, \tag{30}$$

with $\tau_i \equiv \frac{4m_i^2}{m_H^2}$ and the loop functions $A_i(x)$ $(i = 0, 1/2, 1)$ are defined in Appendix B. Notice that the dominant W contribution is $A_1(\tau_W) = -8.32$ for a Higgs mass of 125 GeV, while $A_0(\tau_{h,k}) > 0$, therefore in order to obtain a constructive interference we need to consider negative couplings $\lambda_{hH}, \lambda_{kH}$.

As discussed in Section 2.5, stability of the potential imposes that $2\sqrt{\lambda_H \lambda_x} + \lambda_{xH} > 0$, for $x = h, k$. Since $M_H \sim 125$ GeV fixes the value of the Higgs self-coupling to $\lambda_H \sim 0.13$, it is immediately apparent that large and negative λ_{xH} couplings are going to be in conflict with stability of the potential, unless we push λ_x close to the naive perturbative limit ($\lambda_x < 4\pi$), for which $-3 \lesssim \lambda_{hH}, \lambda_{kH}$. Notice that this fact is not a special feature of the ZB model, but a generic problem of any scenario in which the enhancement of the Higgs diphoton decay rate is due to a virtual charged scalar.

We can consider three different cases:

- If $m_h \ll m_k$,
$$R^h_{\gamma\gamma} \approx \left|1 + \delta R(m_h, \lambda_{hH})\right|^2; \tag{31}$$
- If $m_k \ll m_h$,
$$R^k_{\gamma\gamma} \approx \left|1 + 4\delta R(m_k, \lambda_{kH})\right|^2; \tag{32}$$

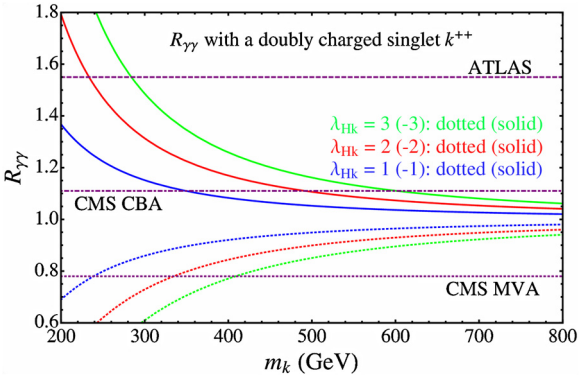

Fig. 3. $R_{\gamma\gamma}$ in the presence of a doubly charged particle. Both an enhancement (as seen by ATLAS [44]) or a suppression (as seen by CMS [45]), can be accommodated. For the same masses and couplings, the singly-charged produces a smaller enhancement/suppression than the doubly-charged, due to its smaller charge.

- If $m_h \approx m_k \equiv m_S$, with

$$R^S_{\gamma\gamma} \approx \left|1 + \delta R(m_S, \lambda_{hH}) + 4\,\delta R(m_S, \lambda_{kH})\right|^2. \tag{33}$$

For the same masses and couplings of both singlets, the doubly charged produces a larger enhancement/suppression than the singly-charged, due to its greater charge.

The largest enhancement can happen when both charged scalars are about the same mass and these masses are low enough. We show in Fig. 3 the prediction of the ratio $R_{\gamma\gamma}$ when the doubly charged scalar k dominates, for different values of the coupling with the Higgs, λ_{kH}. Both an enhancement (as seen by ATLAS [44]) or a suppression (as seen by CMS [45]), can be accommodated. In fact, deviations from the SM value are expected, i.e., $R_{\gamma\gamma} \neq 1$, in particular for below the TeV scale singlets and sizeable scalar couplings. Of course, even for light singlets it is possible that $R_{\gamma\gamma} \approx 1$, either because the relevant scalar couplings are tiny or due to a cancellation between the contributions of the singly charged and the doubly charged scalars.

In principle, the enhancement $R_{\gamma\gamma}$ induced by a singly charged scalar h of similar mass and coupling to the Higgs $\lambda_{hH} \sim \lambda_{kH}$ is smaller; however since the lower limit on m_h from LEP II direct searches is weaker $m_h > 100$ GeV, as discussed in the previous section, and the largest contribution occurs for lower masses, the resulting values of $R_{\gamma\gamma}$ for the allowed range of m_h are comparable to the doubly charged case.

We show in Fig. 4 the contours of $R_{\gamma\gamma} = 1.55$ (0.78), motivated by the experimental results of ATLAS and CMS [44,45], in the plane of the singly and doubly charged masses, for various negative (positive) couplings. In summary, to obtain $R_{\gamma\gamma} \sim 1.5$ we need $m_h \lesssim 200$ GeV and/or $m_k \lesssim 300$ GeV. As it will be shown in the numerical analysis section, these scalar masses are in tension with describing neutrino oscillation data and being compatible with current low-energy bounds in the ZB model if naturality is required at the level of $\kappa = 1$, especially for the NH spectrum. Moreover, the large negative values of the couplings $\lambda_{xH} \sim -2$ required to obtain such enhancement also induce vacuum instability of the ZB scalar potential, unless the corresponding coupling λ_x is close to the perturbative limit, $\lambda_x \sim 8$.

There is a correlation between $H \to \gamma\gamma$ and $H \to Z\gamma$ [46,49,50]. The ratio of the $H \to Z\gamma$ decay rate in the ZB model with respect to the SM one is:

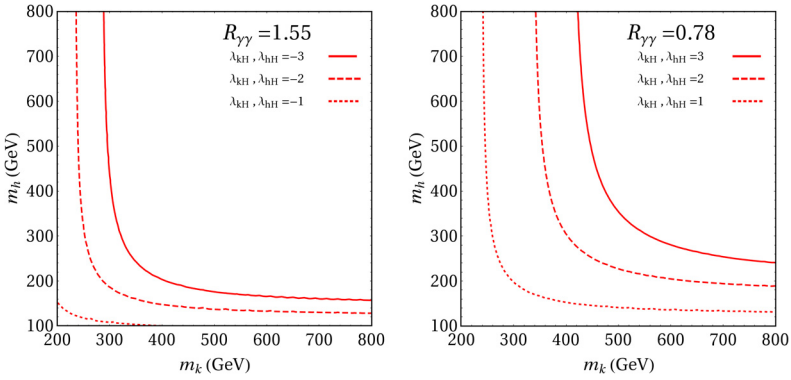

Fig. 4. Contour of $R_{\gamma\gamma} = 1.55$ (left) [44] and $R_{\gamma\gamma} = 0.78$ (right) [45] in the presence of a singly charged and doubly charged particle with the same couplings.

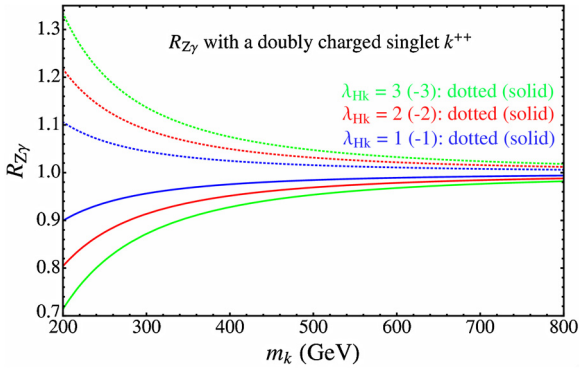

Fig. 5. $R_{\gamma Z}$ in the presence of a doubly charged particle. As can be seen, $H \to Z\gamma$ is anticorrelated with respect to $H \to \gamma\gamma$.

$$R_{Z\gamma} = \frac{\Gamma(H \to Z\gamma)_{ZB}}{\Gamma(H \to Z\gamma)_{SM}} = \left| 1 - g_{Zhh} \frac{\lambda_{hH}\, v^2}{m_h^2} \frac{A_0(\tau_h, \lambda_h)}{\mathcal{A}_{SM}^{Z\gamma}} - g_{Zkk} \frac{2\lambda_{kH}\, v^2}{m_k^2} \frac{A_0(\tau_k, \lambda_k)}{\mathcal{A}_{SM}^{Z\gamma}} \right|^2, \tag{34}$$

where $\mathcal{A}_{SM}^{Z\gamma}$ is the SM $H \to Z\gamma$ decay amplitude,

$$\mathcal{A}_{SM}^{Z\gamma} = \cot\theta_W A_1(\tau_W, \lambda_W) + 6Q_t \frac{T_3^t - 2Q_t s_W^2}{s_W c_W} A_{1/2}(\tau_t, \lambda_t), \tag{35}$$

with $\lambda_i \equiv \frac{4m_i^2}{m_Z^2}$, and the Z boson couplings to the new charged scalars are $g_{Zxx} = -Q_x \cot\theta_W$, $x = h, k$. The loop functions $A_i(x, y)$ $(i = 0, 1/2, 1)$ can be found in Appendix B.

In fact, to have an enhancement in the $H \to \gamma\gamma$ channel, we need negative couplings of the singlets with the Higgs, which in turn implies that the $H \to Z\gamma$ channel is reduced with respect to SM prediction, as can be seen in Fig. 5.

4. Analytical estimates

In this section we give some order of magnitude estimates of the free parameters in the ZB model, which complement and help to understand our full numerical analysis. In particular, we want to estimate to which extent light charged scalar masses, for instance like those required to fit an enhanced Higgs diphoton decay rate or to have a chance of being discovered at the LHC, are consistent with neutrino oscillation data and low-energy constraints.

As discussed in Section 2, with respect to the SM the ZB model has 17 extra parameters relevant for neutrino masses (9 moduli and 5 phases from the Yukawa couplings f, g, and 3 mass parameters from the charged scalar sector, m_h, m_k and μ), plus 5 quartic couplings in the scalar potential. However, some of the free parameters can be traded by the measured neutrino masses and mixings, ensuring in this way that the experimental data is reproduced and reducing the number of free variables as follows.

Since $\det f = 0$, there is an eigenvector $\mathbf{a} = (f_{\mu\tau}, -f_{e\tau}, f_{e\mu})$ which corresponds to the zero eigenvalue, $f\mathbf{a} = 0$ [10]. Then, by exploiting the fact that $\mathbf{a}$ is also an eigenvector of $\mathcal{M}_\nu$, we have

$$D_\nu U^T \mathbf{a} = 0, \tag{36}$$

which leads to three equations, one of which is trivially satisfied because one element of D_ν is zero. The other two equations allow to write the ratios of Yukawa couplings f_{ij} in terms of the neutrino mixing angles and Dirac phase as follows:

$$\begin{aligned}
\frac{f_{e\tau}}{f_{\mu\tau}} &= \tan\theta_{12}\frac{\cos\theta_{23}}{\cos\theta_{13}} + \tan\theta_{13}\sin\theta_{23}e^{-i\delta}, \\
\frac{f_{e\mu}}{f_{\mu\tau}} &= \tan\theta_{12}\frac{\sin\theta_{23}}{\cos\theta_{13}} - \tan\theta_{13}\cos\theta_{23}e^{-i\delta},
\end{aligned} \tag{37}$$

in the NH case, and

$$\begin{aligned}
\frac{f_{e\tau}}{f_{\mu\tau}} &= -\frac{\sin\theta_{23}}{\tan\theta_{13}}e^{-i\delta}, \\
\frac{f_{e\mu}}{f_{\mu\tau}} &= \frac{\cos\theta_{23}}{\tan\theta_{13}}e^{-i\delta},
\end{aligned} \tag{38}$$

for IH spectrum. Therefore, we choose $f_{\mu\tau}$ as a free, real, parameter and obtain (complex) $f_{e\mu}$ and $f_{e\tau}$ from the above equations. Notice that the measured values, $s^2_{12} \sim 0.3$, $s^2_{23} \sim 0.4$ and $s^2_{13} \sim 0.02$ imply that, for NH, the first term on the right-hand side of Eqs. (37) dominates and leads to $f_{e\mu} \sim f_{\mu\tau}/2 \sim f_{e\tau}$. Conversely, for IH it is clear that $f_{e\tau}/f_{e\mu} = -\tan\theta_{23} \sim -1$ and $|f_{e\mu}/f_{\mu\tau}| \sim |f_{e\tau}/f_{\mu\tau}| \sim 4$. Of course, to explain such fine-tuned relations of Yukawa couplings a complete theory of flavor would be needed, which is beyond the scope of this work.

Regarding the Yukawa couplings g, we keep $g_{ee}, g_{e\mu}$ and $g_{e\tau}$ as free complex parameters and fix the remaining ones $(g_{\mu\mu}, g_{\mu\tau}, g_{\tau\tau})$ by imposing the equality of the three elements m_{22}, m_{23} and m_{33} of the neutrino mass matrix $\mathcal{M}_\nu$, written in terms of the parameters of the ZB model in Eq. (13), and in terms of the masses and mixings measured in neutrino oscillation experiments in Eq. (14), i.e.,

$$m_{ij} = \left(U D_\nu U^T\right)_{ij} = \zeta f_{ia}\omega_{ab}f_{jb}, \tag{39}$$

where we have defined $\omega_{ab} \equiv m_a g^*_{ab} m_b$, and $\zeta = \frac{\mu}{48\pi^2 M^2}\tilde{I}(r)$, being r the ratio of the scalar masses, $r \equiv m_k^2/m_h^2$.

Because of the hierarchy among the charged lepton masses, $m_e \ll m_\mu, m_\tau$, it is natural to assume that $\omega_{ee}, \omega_{e\mu}, \omega_{e\tau} \ll \omega_{\mu\mu}, \omega_{\mu\tau}, \omega_{\tau\tau}$. Within the approximation $\omega_{ea} = 0$, Eq. (39) for neutrino masses is simplified, and we can easily estimate the ranges of parameters consistent with neutrino oscillation data. Thus in this section we neglect them, although we keep all ω_{ab} in the full numerical analysis.[6] We then have

$$m_{22} \simeq \zeta f_{\mu\tau}^2 \omega_{\tau\tau}, \qquad m_{23} \simeq -\zeta f_{\mu\tau}^2 \omega_{\mu\tau}, \qquad m_{33} \simeq \zeta f_{\mu\tau}^2 \omega_{\mu\mu}. \tag{40}$$

From the large atmospheric angle we expect

$$|\omega_{\tau\tau}| \simeq |\omega_{\mu\tau}| \simeq |\omega_{\mu\mu}|, \tag{41}$$

which leads to a definite hierarchy among the corresponding g_{ab} couplings:

$$g_{\tau\tau} : g_{\mu\tau} : g_{\mu\mu} \sim m_\mu^2/m_\tau^2 : m_\mu/m_\tau : 1. \tag{42}$$

It is now convenient to write the mass matrix elements m_{ij} in terms of the neutrino masses and mixings. In the normal hierarchy case this gives

$$\begin{aligned}
\zeta f_{\mu\tau}^2 \omega_{\tau\tau} &\simeq m_3 c_{13}^2 s_{23}^2 + m_2 e^{i\phi}\left(c_{12}c_{23} - e^{i\delta}s_{12}s_{13}s_{23}\right)^2, \\
\zeta f_{\mu\tau}^2 \omega_{\mu\tau} &\simeq -m_3 c_{13}^2 c_{23}s_{23} + m_2 e^{i\phi}\left(c_{12}s_{23} + e^{i\delta}c_{23}s_{12}s_{13}\right)\left(c_{12}c_{23} - e^{i\delta}s_{12}s_{13}s_{23}\right), \\
\zeta f_{\mu\tau}^2 \omega_{\mu\mu} &\simeq m_3 c_{13}^2 c_{23}^2 + m_2 e^{i\phi}\left(c_{12}s_{23} + e^{i\delta}c_{23}s_{12}s_{13}\right)^2,
\end{aligned} \tag{43}$$

which for $m_3 \simeq 0.05$ eV and $m_2 \simeq 0.009$ eV, leads to

$$\zeta f_{\mu\tau}^2 |\omega_{ab}| \simeq 0.025 \text{ eV}, \quad a, b = \mu, \tau, \tag{44}$$

in agreement with the expectations of Eq. (41).

In the inverted hierarchy case, Eqs. (40) read

$$\begin{aligned}
\zeta f_{\mu\tau}^2 \omega_{\tau\tau} &\simeq m_1\left(c_{23}s_{12} + e^{i\delta}c_{12}s_{13}s_{23}\right)^2 + m_2 e^{i\phi}\left(c_{12}c_{23} - e^{i\delta}s_{12}s_{13}s_{23}\right)^2, \\
\zeta f_{\mu\tau}^2 \omega_{\mu\tau} &\simeq m_1\left(s_{12}s_{23} - e^{i\delta}c_{12}c_{23}s_{13}\right)\left(c_{23}s_{12} + e^{i\delta}c_{12}s_{13}s_{23}\right) \\
&\quad + m_2 e^{i\phi}\left(c_{12}s_{23} + e^{i\delta}c_{23}s_{12}s_{13}\right)\left(c_{12}c_{23} - e^{i\delta}s_{12}s_{13}s_{23}\right), \\
\zeta f_{\mu\tau}^2 \omega_{\mu\mu} &\simeq m_1\left(s_{12}s_{23} - e^{i\delta}c_{12}c_{23}s_{13}\right)^2 + m_2 e^{i\phi}\left(c_{12}s_{23} + e^{i\delta}c_{23}s_{12}s_{13}\right)^2,
\end{aligned} \tag{45}$$

where $m_1 \simeq m_2 \simeq 0.05$ eV. It is important to notice that for $e^{i\phi} \sim e^{i\delta} \sim 1$ the matrix elements m_{ij} are of the same order as in the NH spectrum, i.e.,

$$\zeta f_{\mu\tau}^2 |\omega_{ab}| \simeq 0.025 \text{ eV}, \quad a, b = \mu, \tau, \tag{46}$$

and therefore the hierarchy of couplings in Eq. (42) is also obtained. However, in the IH case there is a strong cancellation for Majorana phases close to π, so we can obtain smaller values of ω_{ab}. In particular, for $\phi = \delta = \pi$ and the best fit values of the masses and mixing angles we find

$$\zeta f_{\mu\tau}^2 |\omega_{\mu\mu}| \simeq 0.003 \text{ eV}, \tag{47}$$

[6] We find that, in general, this is a very good approximation.

which allows for a smaller $g_{\mu\mu}$ and, as a consequence, a lighter m_k still consistent with the experimental limits. On the contrary, if $\phi \sim \pi$ and $\delta \sim 0$, $|\omega_{\tau\tau}|$ can be very small and therefore $g_{\tau\tau} \ll (m_\mu^2/m_\tau)^2\, g_{\mu\mu}$, although this cancellation has no phenomenological impact. Therefore, although in the following analytic approximations we assume the hierarchy of couplings in Eq. (42), one has to keep in mind that a larger parameter space is expected to be allowed when $\phi \simeq \delta \simeq \pi$. Indeed we will confirm in the full numerical analysis of Section 5 that this region is specially favored for light m_k.

Now we can estimate the lowest scalar masses able to reproduce current neutrino data. Using the neutrino mass equation we can write[7]

$$\frac{m_{33}}{0.05\ \text{eV}} \simeq 500 |g_{\mu\mu}||f_{\mu\tau}|^2 \frac{\mu}{M}\frac{\text{TeV}}{M}\tilde{I}(r). \tag{48}$$

The upper bound on $\tau \to 3\mu$ decay implies that $|g_{\mu\mu}| \lesssim 0.4\ (m_k/\text{TeV})$, while the new MEG limits on $\mu \to e\gamma$ lead to $\epsilon |f_{\mu\tau}|^2 \lesssim 1.3 \cdot 10^{-3}\ (m_h/\text{TeV})^2$, where $\epsilon \equiv |f_{e\tau}/f_{\mu\tau}| \sim 1/2$ (4) for NH (IH). Substituting these constraints in Eq. (48) we obtain

$$\frac{m_{33}}{0.05\,\text{eV}} \lesssim 0.26\, \frac{\mu\, m_k}{\epsilon\, M^2}\left(\frac{m_h}{\text{TeV}}\right)^2 \tilde{I}(r), \tag{49}$$

which can be translated into a lower bound on the scalar masses. Using that $m_{33} \sim 0.025$ eV from neutrino oscillation data, if $m_h > m_k$ then $\mu \leq \kappa\, m_k$ and $\tilde{I}(r) \sim 1$, so Eq. (49) implies that

$$m_h > m_k \gtrsim \frac{1\ \text{TeV}}{\sqrt{\kappa}} \quad \text{NH}, \tag{50}$$

$$m_h > m_k \gtrsim \frac{3\ \text{TeV}}{\sqrt{\kappa}} \quad \text{IH}. \tag{51}$$

On the contrary, if $m_h < m_k$, we find

$$m_k > m_h \gtrsim \sqrt{\frac{m_k}{m_h \kappa \tilde{I}(r)}}\, 1\ \text{TeV} \quad \text{NH}, \tag{52}$$

$$m_k > m_h \gtrsim \sqrt{\frac{m_k}{m_h \kappa \tilde{I}(r)}}\, 3\ \text{TeV} \quad \text{IH}. \tag{53}$$

From the above results,[8] we conclude that:

1. It is easier to reconcile an enhanced Higgs diphoton decay rate with neutrino oscillation data if the former is due to the doubly charged scalar loop contribution, since the lower bounds from neutrino masses are similar, while the BR($H \to \gamma\gamma$) can be accounted for by a heavier m_k. Moreover, if the enhancement is due to a light m_h, then m_k cannot be very heavy, because otherwise neutrino masses are too small.

[7] Notice that similar limits are derived from any of the 23 block elements of $\mathcal{M}_\nu$ when assuming the hierarchy of the g couplings given in Eq. (42).

[8] Our limits in the IH case differ from those in [11]. We traced this difference to the fact that in the estimates of [11] the perturbativity bound $|g_{\mu\mu}| < 1$ is imposed, but for low masses, $m_k < 2$ TeV, such bound is always satisfied, and the relevant bound is $|g_{\mu\mu}| \lesssim 0.4\ (m_k/\text{TeV})$, which depends on m_k and changes the scaling with ϵ, leading to a weaker lower bound on the charged scalar masses in our case. We thank Martin Hirsch for discussions about this point.

Table 4
Allowed ranges for the parameter scan (Neutrino oscillation parameters are obtained from [51–53]).

Parameter	Allowed range
Δ_S	$(7.50 \pm 0.19) \times 10^{-5}$ eV^2
Δ_A	$(2.45 \pm 0.07) \times 10^{-3}$ eV^2
$\sin^2\theta_{12}$	0.30 ± 0.13
$\sin^2\theta_{23}$	$(0.42 \pm 0.04) \cup (0.60 \pm 0.04)$
$\sin^2\theta_{13}$	0.023 ± 0.002
δ, ϕ	$[0, 2\pi]$
$\arg(g_{ee})$, $\arg(g_{e\mu})$, $\arg(g_{e\tau})$	$[0, 2\pi]$
$f_{\mu\tau}$, $\lvert g_{ee}\rvert$, $\lvert g_{e\mu}\rvert$, $\lvert g_{e\tau}\rvert$	$[10^{-7}, 5]$
m_h	$[100, 2 \times 10^3]$ GeV
m_k	$[200, 2 \times 10^3]$ GeV
μ	$[1, 2\kappa \times 10^3]$ GeV

2. For an NH neutrino mass spectrum, it is possible to fit simultaneously neutrino oscillation data, lepton flavor violation constraints and an enhanced BR($H \to \gamma\gamma$) only if the trilinear coupling μ is large, namely $\kappa \gtrsim 4$ (10) for $\min(m_h, m_k) = 500$ (300) GeV, respectively.
3. In general, the case of IH neutrino masses is in conflict with an enhanced Higgs diphoton rate unless $\kappa \sim \mathcal{O}(30)$. However if we take into account the strong cancellations in $\omega_{\mu\mu}$ when $\phi \simeq \delta \simeq \pi$, and allow for a smaller $m_{33} \sim 0.003$ eV, it is also possible to fit all data with $\kappa \sim 4$.

5. Numerical analysis

In order to explore exhaustively the highly multi-dimensional parameter space of the ZB model, naive grid scans are completely inappropriate, the method of choice is resorting to Monte Carlo driven Markov Chains (MCMC) that incorporate all the current experimental information described in precedence. As parameters we will use $\{s^2_{ij}, \Delta_A, \Delta_S, \delta, \phi, f_{\mu\tau}, m_h, m_k, \mu, g_{ee}, g_{e\mu}, g_{e\tau}\}$, and we allow them to vary within the ranges showed in Table 4.

Had we tried to use our MCMC to obtain a posteriori probability distribution functions with a canonical Bayesian meaning, the choice of priors would have had a significant role. Nevertheless, since our aim is to explore where in parameter space could the ZB model adequately reproduce experimental data without weighting in the available parameter space volume (that is, the "metric" in parameter space given by the priors), we will represent instead profiles of highest likelihood (equivalently profiles of minimal $\chi^2 \equiv -2\ln\mathcal{L}$ with $\mathcal{L}$ the likelihood) which, on the contrary, can be interpreted on a frequentist basis. This is not a choice that we make because of the merits or demerits of either statistical school: our goal remains to understand if and where the ZB "works well", i.e. could fit experimental data. The interpretation of the results/plots will be clear: they show the regions where the model is in agreement with data without regard to their size when the remaining information (parameters and observables) is marginalized over.[9] In this case, exploring the parameter space in a uniform, logarithmic or other manner, in some given

[9] Typically both approaches should converge to similar results when (experimental) information abounds; in a study such as this one, if they differ, rather than sticking to one or the other, from the physical point of view we would only conclude that the current experimental data is not yet sufficient to pin down or exclude the model.

parameter will not affect our results (only the computational efficiency required to reach them will be, of course, affected).

For the modeling of experimental data we typically resort to individual Gaussian likelihoods for measured quantities. Bounds are implemented through smooth likelihood functions that include, piecewise, a constant and a Gaussian-like behavior. For the sake of clarity: if the experimental bound for a given observable $\mathcal{O}$ is $B^{\mathcal{O}}_{[90\%\ \mathrm{C.L.}]}$ at 90% C.L. (1.64σ in one dimension), the χ^2 contribution associated to the model prediction $\mathcal{O}_{\mathrm{th}}$ for this observable is

$$\chi^2(\mathcal{O}_{\mathrm{th}}) = \begin{cases} 0, & \mathcal{O}_{\mathrm{th}} < B^{\mathcal{O}}_{[90\%\ \mathrm{C.L.}]}/1.64, \\ \left(\frac{1.64\mathcal{O}_{\mathrm{th}}}{B^{\mathcal{O}}_{[90\%\ \mathrm{C.L.}]}} - 1\right)^2 \left(\frac{1.64}{0.64}\right)^2, & \mathcal{O}_{\mathrm{th}} \geq B^{\mathcal{O}}_{[90\%\ \mathrm{C.L.}]}/1.64. \end{cases}$$

In this way we avoid imposing sharp stepwise bounds or half-Gaussian with the best value at zero that may penalize deviating from null predictions when this might not be supported by experimental evidence (in particular when the number of bounds included in the analysis is significant).

Simulations are done for both normal and inverted hierarchy. In each point of the parameter space we compute the full χ^2, including all measurements and bounds. In the plots we show the regions with the total $\Delta\chi^2 \leq 6$, which correspond to 95% confidence levels with two variables.

To compare our results with the analysis presented a few years ago by some of us [12] some remarks are in order: first, here we have updated the experimental input on LFV and neutrino oscillation parameters, as well as LHC direct searches. The new limits, in particular on $\mu \to e\gamma$, tend to reduce the allowed regions but not dramatically. Especially important is the determination of $\sin\theta_{13}$: as shown in [12], already before its measurement the ZB model predicted a large mixing angle θ_{13} in the case of IH spectrum, close to the previous experimental upper limit, while for NH any value of θ_{13} below the bound was allowed. In fact, a very small value of θ_{13} would have ruled out the IH possibility within the ZB model. Second, although the scanning of parameters is performed like in [12], we have chosen here to present results in terms of profiles of the highest likelihood, which are insensitive to the volume of the parameter space and the priors used to scan it. This allows us to explore regions where parameters are fine tuned (after all, Yukawa couplings always require a certain degree of fine tuning). This is important since, as we have seen, the model is highly constrained at present and less conservative assumptions could exclude it before time, at least in the region of low masses. Moreover, we focus only on the region of masses with phenomenological interest ($m_{h,k} < 2$ TeV) precisely to explore better the region of low masses.

In Fig. 6 we depict the points allowed by neutrino oscillation data and all low energy constraints in the plane (m_h, m_k) for the two mass orderings (NH and IH) and different values of the fine-tuning parameter in Eq. (9) ($\kappa = 1$ darker, $\kappa = 5$ dark, $\kappa = 4\pi$ light). The results of the numerical analysis imply that in general the indirect lower bounds on m_h and m_k from neutrino oscillation data and low energy constraints are stronger than the current limits from direct searches, except when cancellations occur for $\delta, \phi \sim \pi$, especially in the IH case, and/or when naturality assumptions on μ are relaxed, allowing for $\kappa = 4\pi$. In Table 5 we summarize the lower bounds on the scalar masses obtained for the three values of the naturality parameter κ, and two illustrative values of the Dirac phase, $\delta = 0, \pi$. For $\delta \sim -\pi/2$, as might be suggested by a recent analysis [51], the bounds are slightly weaker than in the $\delta = 0$ case (see Fig. 7).

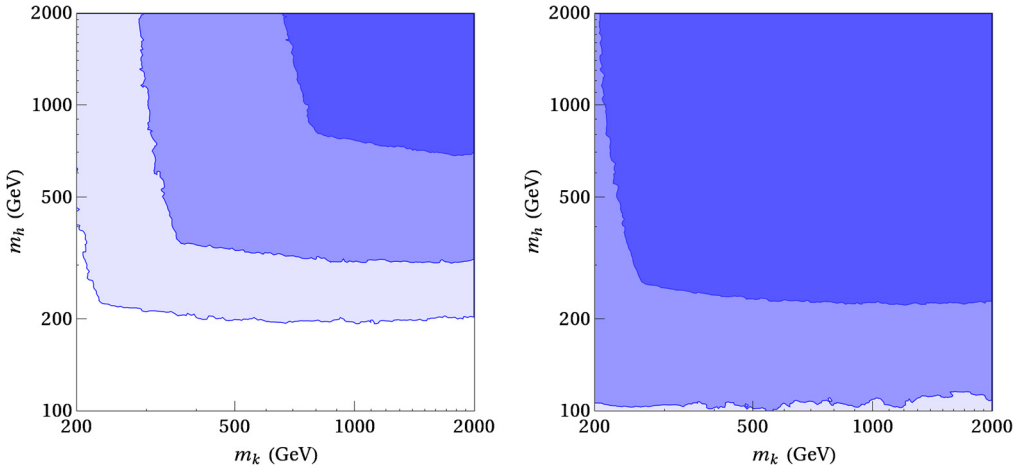

Fig. 6. m_h vs m_k for NH (left) and IH (right) for different values of the perturbative parameter $\kappa = 1, 5, 4\pi$ (dark to light colors).

Table 5
Lower bounds for the scalar masses for NH and IH and the naturality constraints parametrized by the three values of κ. We present results for $\delta = \pi$ ($\delta = 0$) (see Figs. 6 and 7).

κ	NH			IH		
	1	5	4π	1	5	4π
m_h (GeV)	700 (1000)	300 (400)	200 (250)	220 (>2000)	100 (1000)	100 (650)
m_k (GeV)	700 (1100)	300 (450)	200 (250)	200 (>2000)	200 (1000)	200 (550)

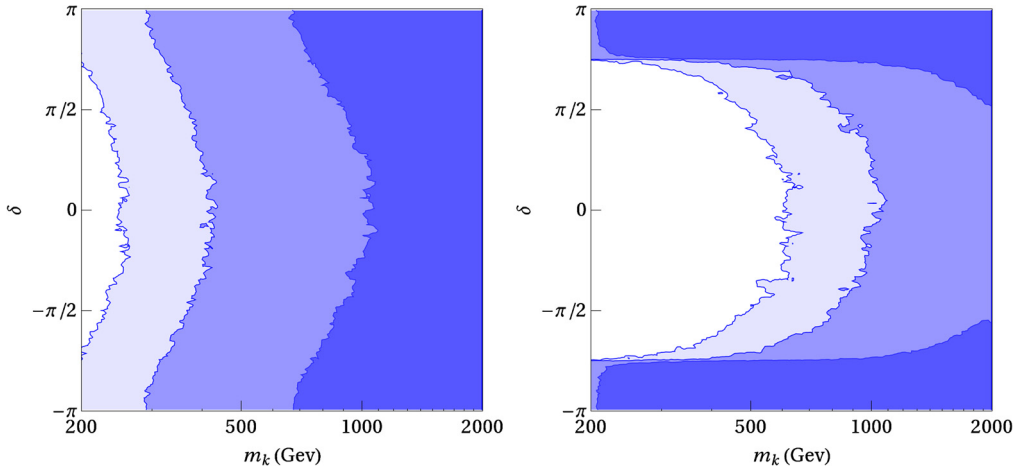

Fig. 7. δ vs m_k in NH (left) and IH (right).

The correlation between the CP phase δ of the neutrino mixing matrix and the scalar masses is illustrated in Fig. 7, where we plot δ versus the doubly charged scalar mass, m_k.[10] Such

[10] The correlation of δ with m_h is entirely analogous.

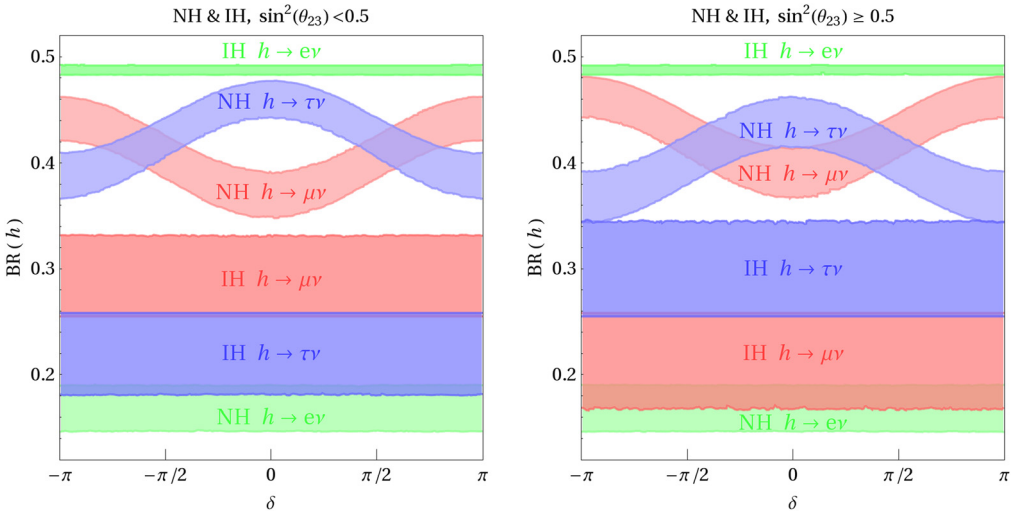

Fig. 8. Branching ratios of the charged singlet h to $e\nu$, $\mu\nu$, $\tau\nu$ splitting the two currently allowed octants of θ_{23}, $\theta_{23} < 45°$ ($\theta_{23} > 45°$) left (right). One can see the dependence on δ for the NH spectrum in the $\mu\nu$ and $\tau\nu$ channels. The most significant change between octants is the interchange of the $\mu\nu$ and $\tau\nu$ for the IH case. The bands are 95% C.L. regions.

correlation is especially relevant in the IH case, where scalar masses lower than $\sim$1 TeV are only allowed if $\delta \sim \pi$. A similar correlation with the phase ϕ was already found in [12] for IH spectrum, so we do not show it here.

Regarding the singly charged scalar $h^{\pm}$, the width of its decay modes ($e\nu$, $\mu\nu$, $\tau\nu$) is fixed by the f_{ia} couplings to leptons (see for instance [11,12] for the relevant formulae). Therefore, after the measurement of θ_{13}, present neutrino oscillation data determine completely the BRs of h from Eqs. (37) and (38), up to a residual dependence on the CP phase δ in the case of NH spectrum. In this case, a very precise measurement of the branching ratios in the $\mu\nu$ or $\tau\nu$ channels (probably in a next generation collider) will predict the CP phase δ, and vice versa. We show the ranges attainable by the different BRs in Fig. 8, as a function of δ, splitting the two currently allowed octants of θ_{23}. The most significant change between octants is the interchange of the $\mu\nu$ and $\tau\nu$ for the IH case. Clearly, the best option to discriminate between hierarchies is the $e\nu$ channel.

An important point of the ZB model is that the doubly charged scalar can decay to two singly charged scalars, which are difficult to detect at the LHC. However, in Fig. 6 we see that for an NH neutrino mass spectrum $m_h > 200$ GeV, and the channel $k \to hh$ is closed for $m_k < 400$ GeV. Therefore, present bounds on m_k from dilepton searches at LHC discussed in Section 2.4 apply. For the IH case, the $k \to hh$ channel is always open and can be dominant, unless $\kappa = 1$, for which we obtain that it is closed in the region $m_k < 440$ GeV. Thus in general current direct bounds from LHC are weaker.

Let us now turn to the g_{ab} couplings. We find always $g_{\tau\tau} \ll g_{\mu\tau}$, both for the NH and IH cases, in agreement with the analytic estimates in Eq. (42); however the expected ratio $g_{\mu\mu}/g_{\mu\tau} \sim m_\tau/m_\mu$ is only fulfilled for the NH spectrum, since in the IH case large cancellations when the phases of the PMNS matrix U are $\delta \sim \phi \sim \pi$ lead to smaller $g_{\mu\mu} \ll g_{\mu\tau}$. This can be seen in Fig. 9, where we show the ratios $g_{\tau\tau}/g_{\mu\tau}$ and $g_{\mu\mu}/g_{\mu\tau}$ obtained in the numerical simulation as

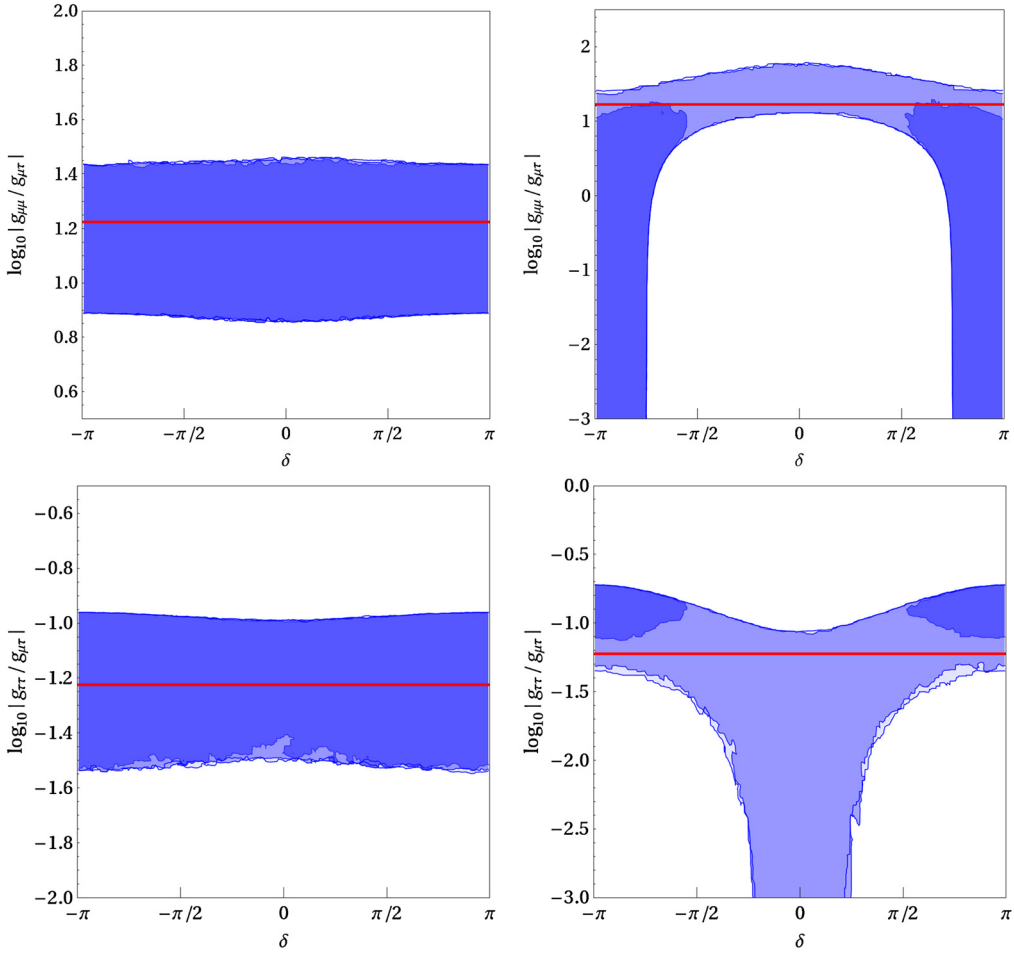

Fig. 9. $\log|g_{\mu\mu}/g_{\mu\tau}|$ and $\log|g_{\tau\tau}/g_{\mu\tau}|$ vs δ for NH (left) and IH (right). The horizontal red lines represent the naive approximation in Eq. (42). (For interpretation of the references to color in this figure, the reader is referred to the web version of this article.)

a function of δ, together with the expectation based on the analytic approximations, which is just a constant fixed by the charged lepton masses (red horizontal line).[11]

To set the absolute scale of the couplings we present in Fig. 10 the value of the largest couplings against m_k, namely $g_{\mu\mu}$ in the NH case, and $g_{\mu\tau}$ in the IH case. We see that in both cases the couplings are always in the range from 10^{-2} to 1 and therefore they tend to dominate the decays of the k^{++}.

Regarding the couplings g_{ea}, which are not determined by the neutrino mass matrix, bounds from LFV charged lepton decays strongly constrain $g_{e\tau}$ and $g_{e\mu}$ to be less than $\mathcal{O}(0.01)$, while g_{ee} can be larger, $\mathcal{O}(1)$. The constraint on $|g_{ee}g_{e\mu}|$ from $\mu \to 3e$ implies that $|g_{ee}g_{e\mu}| < 2.3 \times 10^{-5}\,(m_k/\text{TeV})^2$ and it is illustrated in Fig. 11.

[11] In the NH case there can also be cancellations with the $g_{e\tau}$ terms, which have been neglected in Eq. (43), that would allow much smaller values of $g_{\tau\tau}$ and $g_{\mu\tau}$, but those only occur for $\kappa = 4\pi$ and in a tiny region of the parameter space.

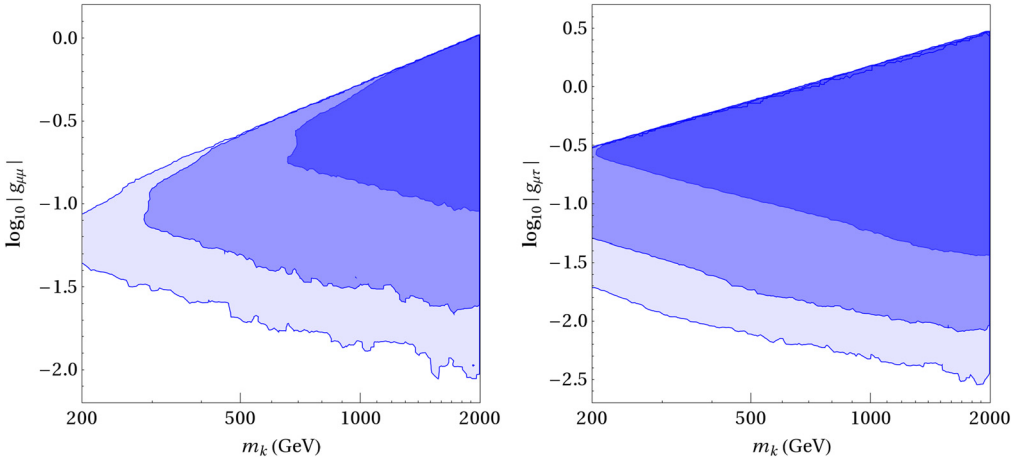

Fig. 10. $\log|g_{\mu\mu}|$ vs m_k for NH (left) and $\log|g_{\mu\tau}|$ vs m_k for IH (right).

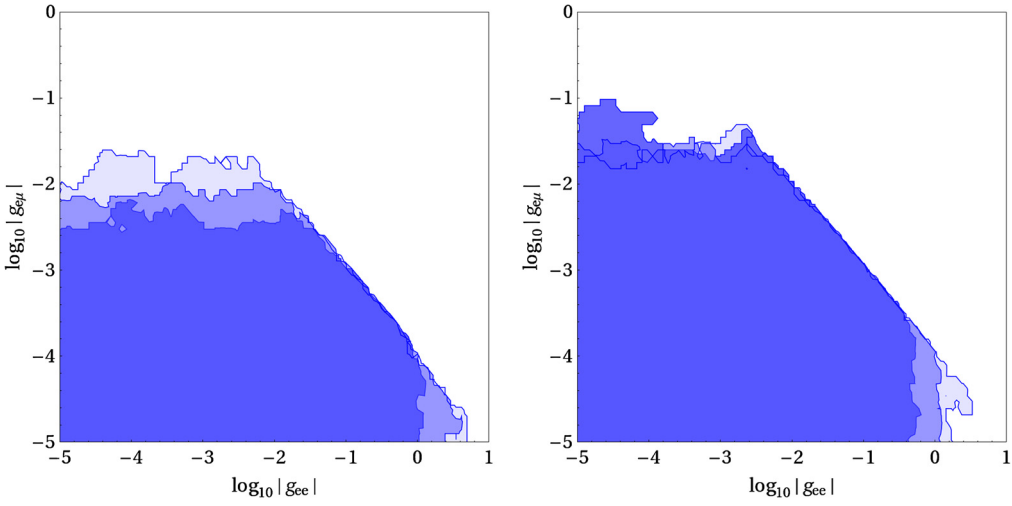

Fig. 11. $\log|g_{e\mu}|$ vs $\log|g_{ee}|$ for NH (left) and IH (right).

Since the widths of the $k^{\pm\pm}$ leptonic decay modes are directly related to these couplings, from the above results we can readily infer the corresponding BRs. We find that the probability of $k \to e\mu, e\tau, \tau\tau$ is always negligible (even in the IH case, $g_{e\mu}$ can be at most 0.1 and only when $\delta \sim \pi$). For $m_k \lesssim 400$ GeV, and NH neutrino spectrum, $\mathrm{BR}(k \to ee) + \mathrm{BR}(k \to \mu\mu) \sim 1$, since the $k \to hh$ decay channel is closed; therefore $k^{\pm\pm}$ cannot evade current LHC bounds on doubly-charged scalar searches and the limit $m_k > 310$ GeV applies (400 GeV if no signal is found at 8 TeV with 20 fb^{-1} [36]). In the same m_k range, for IH neutrino spectrum the $\mathrm{BR}(k \to \mu\tau)$ can also be significant and the channel $k \to hh$ is open (unless $\kappa = 1$, for which it is only open for $m_k > 440$ GeV), thus the present bound is weaker.

When the upcoming LHC 13–14 TeV data is available, it is important to take into account that the decay channel $k \to hh$ is open for $m_k \gtrsim 400$ GeV, and can be dominant, so in this mass range limits on doubly-charged scalars from dilepton searches will not apply to the ZB model. On the

contrary, if a doubly charged scalar were detected at LHC in any mass range, neutrino oscillation data and low energy constraints are powerful enough to falsify the ZB model to a large extent. For instance, we know that $\mathrm{BR}(k \to e\mu, e\tau, \tau\tau)$ are negligible for any neutrino mass spectrum, while a sizeable $\mathrm{BR}(k \to \mu\tau)$ is only compatible with an IH spectrum.

6. Conclusions

We have analyzed the ZB model in the light of recent data: the measured neutrino mixing angle θ_{13}, limits from the rare decay $\mu \to e\gamma$ and LHC results. Although the model contains many free parameters, neutrino oscillation data and low energy constraints are powerful enough to rule out sizeable regions of the parameter space. A large source of uncertainty comes from the mass scale of the new physics, which is unknown. Since we are interested on possible signatures at the LHC, we present results for the masses of the extra scalar fields below 2 TeV. Previous analyses [11,12] have shown that larger mass scales are always allowed, given the absence of significant deviations from the SM besides neutrino masses.

Even within this reduced scenario, there is still a free mass parameter, the trilinear coupling between the charged scalars, μ, which remains mainly unconstrained. Naturality arguments together with perturbativity and vacuum stability bounds indicate that μ cannot be much larger than the physical scalar masses, m_k, m_h, but it is not possible to determine a precise theoretical limit. Because the neutrino masses depend linearly on the parameter μ, the ability of the model to accommodate all present data is quite sensitive to the upper limit allowed for it, so we have considered three limiting values, $\mu < \kappa \min(m_k, m_h)$, with $\kappa = 1, 5, 4\pi$. Within the above ranges for the mass parameters of the ZB model, we have performed an exhaustive numerical analysis using Monte Carlo Markov Chains (MCMC), incorporating all the current experimental information available, both for NH and IH neutrino masses. The results of the analysis are presented in Section 5 and summarized in Figs. 6–11.

We have addressed the possibility that the slight excess in the Higgs diphoton decay observed by the ATLAS Collaboration is due to virtual loops of the extra charged scalars of the ZB model, $h^\pm$ and $k^{\pm\pm}$. Note that in the Zee–Babu model, as the new particles are singlets, there is a negative correlation between $H \to \gamma\gamma$ and $H \to \gamma Z$. Although a similar study has been performed in [22], it was limited to the scalar sector parameters of the model, and neutrino data, which we find crucial to determine the allowed charged scalar masses, was not included in the analysis. In agreement with [22], we find that in order to accommodate an enhanced $H \to \gamma\gamma$ decay rate, large and negative $\lambda_{hH}, \lambda_{kH}$ couplings are needed, together with light scalar masses $m_h < 200$ GeV, $m_k < 300$ GeV. Such couplings are in conflict with the stability of the potential, unless the self-couplings $\lambda_{h,k}$ are pushed close to the naive perturbative limit, $\sim 4\pi$. As a consequence, even if vacuum stability and perturbativity constraints are satisfied at the electroweak scale, RGE running leads to non-perturbative couplings at scales not far from the electroweak scale, as shown in Fig. 2.

When neutrino data and low energy constraints are taken into account, we still find regions of the parameter space in which such enhancement is compatible with all current experimental data; in particular, it seems easier if the enhancement is due to the doubly-charged scalar loop contribution. As can be seen in Fig. 6, in the NH case, the trilinear coupling μ should be near its upper limit, while in the IH case lower masses can be achieved in the region $\delta \sim \phi \sim \pi$ due to cancellations.

Regarding LHC bounds on the doubly-charged scalar mass, they are largely dependent on the BRs of the $k^{\pm\pm}$ decay modes, namely same sign leptons $\ell_a^\pm \ell_b^\pm$ and $h^\pm h^\pm$. The leptonic decay

widths are controlled by the g_{ab} couplings to the right-handed leptons, which are in principle unknown. By imposing that the measured neutrino mass matrix is reproduced, within the approximation $m_e = 0$ one obtains analytically that $g_{\tau\tau} : g_{\mu\tau} : g_{\mu\mu} \sim m_\mu^2/m_\tau^2 : m_\mu/m_\tau : 1$, while there is no information on the g_{ea} couplings. Our numerical analysis confirms the above ratio of couplings in the case of NH, but for the IH spectrum there can be large cancellations if the PMNS matrix phases δ, ϕ are close to π, leading to $g_{\tau\tau} \ll g_{\mu\tau} \sim g_{\mu\mu}$. In both cases, $g_{e\mu}, g_{e\tau} \lesssim 0.1$.

Moreover, in NH, if $m_k < 400$ GeV for $\kappa = 4\pi$ ($m_k < 600$ GeV if $\kappa = 5$), $m_h < m_k/2$ is ruled out, therefore the decay channel $k \to hh$ is kinematically closed and the LHC bounds from doubly-charged scalar searches cannot be evaded. In IH, however, for $\delta \sim \phi \sim \pi$ the $k \to hh$ channel is open unless $\kappa = 1$, while if δ is very different from π, indirect bounds on m_k set a much stronger constraint than direct LHC searches.

As a consequence, if the light neutrino spectrum is NH, k decays mainly to $ee, \mu\mu$, and the current bound from LHC is $m_k > 310$ GeV, while if the spectrum is IH, k may also decay to $\mu\tau$ and hh, so the present bound is weaker, about 200 GeV. Were a doubly-charged boson discovered at LHC, the measurement of its leptonic BRs could rule out the ZB model, or predict a definite neutrino mass spectrum. Conversely, if a CP phase δ is measured in future neutrino oscillation experiments to be quite different from π together with an IH spectrum, the mass of the charged scalars of the ZB model will be pushed up well outside the LHC reach.

Note: During the final stages of this work we became aware of [54], where an analysis of the Zee–Babu model was performed. Our bounds on the scalar masses are comparable to theirs taking into account the slightly different procedures, in particular that they fix the neutrino oscillation parameters to their best fit values and we allow them to vary in their two sigma range. While in our work we focus on prospects for the LHC, in [54] the possibility of detecting the doubly charged singlet in a future linear collider is studied.

Acknowledgements

We are thankful to the authors of [54] for sharing with us their work and for useful discussions. We also thank Marcela Carena, Ian Low and Carlos Wagner for discussions. This work has been partially supported by the European Union FP7 ITN INVISIBLES (Marie Curie Actions, PITN-GA-2011-289442), by the Spanish MINECO under grants FPA2011-23897, FPA2011-29678, Consolider-Ingenio PAU (CSD2007-00060) and CPAN (CSD2007-00042) and by Generalitat Valenciana grants PROMETEO/2009/116 and PROMETEO/2009/128. M.N. is supported by a postdoctoral fellowship of project CERN/FP/123580/2011 at CFTP (PEst-OE/FIS/UI0777/2013), projects granted by *Fundação para a Ciência e a Tecnologia* (Portugal), and partially funded by POCTI (FEDER). J.H.-G. is supported by the MINECO under the FPU program. He would also like to acknowledge NORDITA for their hospitality during the revision of the final version of this work, carried out during the "News in Neutrino Physics" program.

Appendix A. RGEs in the ZB model

$$
\begin{aligned}
16\pi^2\beta_H &= \frac{3}{8}\left[\left(g^2+g'^2\right)^2+2g^4\right]-\left(3g'^2+9g^2\right)\lambda_H+24\lambda_H^2+\lambda_{hH}^2\\
&\quad+\lambda_{kH}^2-6y_t^4+12\lambda_H y_t^2\\
16\pi^2\beta_h &= 6g'^4-12g'^2\lambda_h+20\lambda_h^2+2\lambda_{hH}^2+\lambda_{hk}^2\\
16\pi^2\beta_k &= 96g'^4-48g'^2\lambda_k+20\lambda_k^2+2\lambda_{kH}^2+\lambda_{hk}^2
\end{aligned}
$$

$$
\begin{aligned}
16\pi^2\beta_{hH} &= 3g'^4 - \left(\frac{15}{2}g'^2 + \frac{9}{2}g^2\right)\lambda_{hH} + 12\lambda_H\lambda_{hH} + 8\lambda_h\lambda_{hH} \\
&\quad + 2\lambda_{kH}\lambda_{hk} + 4\lambda_{hH}^2 + 6\lambda_{hH}y_t^2 \\
16\pi^2\beta_{kH} &= 12g'^4 - \left(\frac{51}{2}g'^2 + \frac{9}{2}g^2\right)\lambda_{kH} + 12\lambda_H\lambda_{kH} + 8\lambda_k\lambda_{kH} \\
&\quad + 2\lambda_{hH}\lambda_{hk} + 4\lambda_{kH}^2 + 6\lambda_{kH}y_t^2 \\
16\pi^2\beta_{hk} &= 48g'^4 - 30g'^2\lambda_{hk} + 4\lambda_{kH}\lambda_{hH} + 8\lambda_h\lambda_{hk} + 8\lambda_k\lambda_{hk} + 4\lambda_{hk}^2, \qquad \text{(A.1)} \\
16\pi^2\beta_{g'} &= \frac{5}{3}\left(\frac{41}{10} + 1\right)g'^3 \\
16\pi^2\beta_g &= -\frac{19}{6}g^3 \\
16\pi^2\beta_{g_3} &= -7g_3^3, \qquad \text{(A.2)} \\
16\pi^2\beta_t &= y_t\left\{\frac{9}{2}y_t^2 - \left(\frac{17}{12}g'^2 + \frac{9}{4}g^2 + 8g_3^2\right)\right\}. \qquad \text{(A.3)}
\end{aligned}
$$

Here g_3, g, g' are the SM $SU(3)_C$, $SU(2)_L$ and $U(1)_Y$ gauge couplings, respectively, and we have neglected all the Yukawa couplings but the top quark Yukawa, y_t. We have also neglected the f_{ab}, g_{ab} couplings because for the range of singlet scalar masses that we consider ($\leq$2 TeV), they are severely constrained by LFV and are much smaller than 1 except for some corners of the parameter space where some of them could be order one. For the analysis of the vacuum stability of the scalar potential f_{ab}, g_{ab} are subdominant, specially in the region of large and negative mixed scalar couplings required to accommodate the diphoton excess in Higgs decays. For smaller mixed scalar couplings, however, a more detailed analysis including all Yukawa couplings and taking also into account leading two-loop effects (as well as top quark mass uncertainties for the Higgs quartic coupling) should be carried out, which is beyond the scope of this work.

Appendix B. Loop functions for $H \to \gamma\gamma$ and $H \to Z\gamma$

- Functions relevant for $H \to \gamma\gamma$:

$$A_0(x) = -x + x^2 f\left(\frac{1}{x}\right) \qquad \text{(B.1)}$$

$$A_{1/2}(x) = 2x + 2x(1-x) f\left(\frac{1}{x}\right) \qquad \text{(B.2)}$$

$$A_1(x) = -2 - 3x - 3x(2-x) f\left(\frac{1}{x}\right) \qquad \text{(B.3)}$$

- Functions relevant for $H \to Z\gamma$:

$$A_0(x, y) = I_1(x, y) \qquad \text{(B.4)}$$

$$A_{1/2}(x, y) = I_1(x, y) - I_2(x, y) \qquad \text{(B.5)}$$

$$A_1(x, y) = 4\left(3 - \tan^2\theta_w\right) I_2(x, y) + \left[\left(1 + 2x^{-1}\right)\tan^2\theta_w - \left(5 + 2x^{-1}\right)\right] I_1(x, y) \qquad \text{(B.6)}$$

where

$$I_1(x,y) = \frac{xy}{2(x-y)} + \frac{x^2y^2}{2(x-y)^2}\left[f\left(x^{-1}\right) - f\left(y^{-1}\right)\right] + \frac{x^2y}{(x-y)^2}\left[g\left(x^{-1}\right) - g\left(y^{-1}\right)\right] \tag{B.7}$$

$$I_2(x,y) = -\frac{xy}{2(x-y)}\left[f\left(x^{-1}\right) - f\left(y^{-1}\right)\right] \tag{B.8}$$

and, for a Higgs mass below the kinematic threshold of the loop particle, $m_H < 2m_i$,

$$f(x) = \arcsin^2\sqrt{x}, \tag{B.9}$$

$$g(x) = \sqrt{x^{-1}-1}\arcsin\sqrt{x}. \tag{B.10}$$

References

[1] R. Mohapatra, S. Antusch, K. Babu, G. Barenboim, M.-C. Chen, et al., Theory of neutrinos: a White paper, Rep. Prog. Phys. 70 (2007) 1757–1867, arXiv:hep-ph/0510213, InSPIRE.

[2] M. Gonzalez-Garcia, M. Maltoni, Phenomenology with massive neutrinos, Phys. Rep. 460 (2008) 1–129, arXiv:0704.1800, InSPIRE.

[3] Particle Data Group, J. Beringer, et al., Review of Particle Physics (RPP), Phys. Rev. D 86 (2012) 010001, InSPIRE.

[4] Intensity Frontier Neutrino Working Group, A. de Gouvea, et al., Neutrinos, arXiv:1310.4340, InSPIRE.

[5] A. Zee, Quantum numbers of Majorana neutrino masses, Nucl. Phys. B 264 (1986) 99, InSPIRE.

[6] K. Babu, Model of 'Calculable' Majorana neutrino masses, Phys. Lett. B 203 (1988) 132, InSPIRE.

[7] T. Cheng, L.-F. Li, Neutrino masses, mixings and oscillations in $SU(2) \times U(1)$ models of electroweak interactions, Phys. Rev. D 22 (1980) 2860, InSPIRE.

[8] F. del Aguila, A. Aparici, S. Bhattacharya, A. Santamaria, J. Wudka, A realistic model of neutrino masses with a large neutrinoless double beta decay rate, J. High Energy Phys. 1205 (2012) 133, arXiv:1111.6960, InSPIRE.

[9] F. del Aguila, A. Aparici, S. Bhattacharya, A. Santamaria, J. Wudka, Neutrinoless double β decay with small neutrino masses, PoS Corfu2012 (2013) 028, arXiv:1305.4900, InSPIRE.

[10] K. Babu, C. Macesanu, Two loop neutrino mass generation and its experimental consequences, Phys. Rev. D 67 (2003) 073010, arXiv:hep-ph/0212058, InSPIRE.

[11] D. Aristizabal Sierra, M. Hirsch, Experimental tests for the Babu–Zee two-loop model of Majorana neutrino masses, J. High Energy Phys. 0612 (2006) 052, arXiv:hep-ph/0609307, InSPIRE.

[12] M. Nebot, J.F. Oliver, D. Palao, A. Santamaria, Prospects for the Zee–Babu Model at the CERN LHC and low energy experiments, Phys. Rev. D 77 (2008) 093013, arXiv:0711.0483, InSPIRE.

[13] T. Ohlsson, T. Schwetz, H. Zhang, Non-standard neutrino interactions in the Zee–Babu model, Phys. Lett. B 681 (2009) 269–275, arXiv:0909.0455, InSPIRE.

[14] DOUBLE-CHOOZ Collaboration, Y. Abe, et al., Indication for the disappearance of reactor electron antineutrinos in the Double Chooz experiment, Phys. Rev. Lett. 108 (2012) 131801, arXiv:1112.6353, InSPIRE.

[15] DAYA-BAY Collaboration, F. An, et al., Observation of electron–antineutrino disappearance at Daya Bay, Phys. Rev. Lett. 108 (2012) 171803, arXiv:1203.1669, InSPIRE.

[16] RENO Collaboration, J. Ahn, et al., Observation of reactor electron antineutrino disappearance in the RENO experiment, Phys. Rev. Lett. 108 (2012) 191802, arXiv:1204.0626, InSPIRE.

[17] MEG Collaboration, J. Adam, et al., New constraint on the existence of the $\mu \to e\gamma$ decay, Phys. Rev. Lett. 110 (2013) 201801, arXiv:1303.0754, InSPIRE.

[18] ATLAS Collaboration, G. Aad, et al., Search for doubly-charged Higgs bosons in like-sign dilepton final states at $\sqrt{s} = 7$ TeV with the ATLAS detector, Eur. Phys. J. C 72 (2012) 2244, arXiv:1210.5070, InSPIRE.

[19] CMS Collaboration, S. Chatrchyan, et al., A search for a doubly-charged Higgs boson in pp collisions at $\sqrt{s} = 7$ TeV, Eur. Phys. J. C 72 (2012) 2189, arXiv:1207.2666, InSPIRE.

[20] ATLAS Collaboration, G. Aad, et al., Observation of a new particle in the search for the Standard Model Higgs boson with the ATLAS detector at the LHC, Phys. Lett. B 716 (2012) 1–29, arXiv:1207.7214, InSPIRE.

[21] CMS Collaboration, S. Chatrchyan, et al., Observation of a new boson at a mass of 125 GeV with the CMS experiment at the LHC, Phys. Lett. B 716 (2012) 30–61, arXiv:1207.7235, InSPIRE.

[22] W. Chao, J.-H. Zhang, Y. Zhang, Vacuum stability and Higgs diphoton decay rate in the Zee–Babu model, J. High Energy Phys. 1306 (2013) 039, arXiv:1212.6272, InSPIRE.
[23] D. Dicus, V. Mathur, Upper bounds on the values of masses in unified gauge theories, Phys. Rev. D 7 (1973) 3111–3114, InSPIRE.
[24] B.W. Lee, C. Quigg, H. Thacker, Weak interactions at very high-energies: the role of the Higgs boson mass, Phys. Rev. D 16 (1977) 1519, InSPIRE.
[25] J. Frere, D. Jones, S. Raby, Fermion masses and induction of the weak scale by supergravity, Nucl. Phys. B 222 (1983) 11, InSPIRE.
[26] L. Alvarez-Gaume, J. Polchinski, M.B. Wise, Minimal low-energy supergravity, Nucl. Phys. B 221 (1983) 495, InSPIRE.
[27] J. Casas, S. Dimopoulos, Stability bounds on flavor violating trilinear soft terms in the MSSM, Phys. Lett. B 387 (1996) 107–112, arXiv:hep-ph/9606237, InSPIRE.
[28] K.L. McDonald, B. McKellar, Evaluating the two loop diagram responsible for neutrino mass in Babu's model, arXiv:hep-ph/0309270, InSPIRE.
[29] A. Pich, Precision tau physics, arXiv:1310.7922, InSPIRE.
[30] M. Raidal, A. Santamaria, Muon electron conversion in nuclei versus $mu \to e\gamma$: an effective field theory point of view, Phys. Lett. B 421 (1998) 250–258, arXiv:hep-ph/9710389, InSPIRE.
[31] H. Witte, B. Muratori, K. Hock, R. Appleby, H. Owen, et al., Status of the PRISM FFAG design for the next generation muon-to-electron conversion experiment, Conf. Proc. C1205201 (2012) 79–81, InSPIRE.
[32] COMET Collaboration, Y. Kuno, A search for muon-to-electron conversion at J-PARC: the COMET experiment, PTEP, Proces. Teh. Energ. Poljopr. 2013 (2013) 022C01, InSPIRE.
[33] mu2e Collaboration, G. Onorato, The Mu2e experiment at Fermilab: $\mu^- N \to e^- N$, Nucl. Instrum. Methods A 718 (2013) 102–103, InSPIRE.
[34] F. del Aguila, A. Aparici, S. Bhattacharya, A. Santamaria, J. Wudka, Effective Lagrangian approach to neutrinoless double beta decay and neutrino masses, J. High Energy Phys. 1206 (2012) 146, arXiv:1204.5986, InSPIRE.
[35] J. Tang, W. Winter, Physics with near detectors at a neutrino factory, Phys. Rev. D 80 (2009) 053001, arXiv:0903.3039, InSPIRE.
[36] F. del Aguila, M. Chala, LHC bounds on lepton number violation mediated by doubly and singly-charged scalars, arXiv:1311.1510, InSPIRE.
[37] H. Sugiyama, K. Tsumura, H. Yokoya, Discrimination of models including doubly charged scalar bosons by using tau lepton decay distributions, Phys. Lett. B 717 (2012) 229–234, arXiv:1207.0179, InSPIRE.
[38] F. del Aguila, M. Chala, A. Santamaria, J. Wudka, Discriminating between lepton number violating scalars using events with four and three charged leptons at the LHC, Phys. Lett. B 725 (2013) 310–315, arXiv:1305.3904, InSPIRE.
[39] F. del Aguila, M. Chala, A. Santamaria, J. Wudka, Distinguishing between lepton number violating scalars at the LHC, arXiv:1307.0510, InSPIRE.
[40] M. Muhlleitner, M. Spira, A note on doubly charged Higgs pair production at hadron colliders, Phys. Rev. D 68 (2003) 117701, arXiv:hep-ph/0305288, InSPIRE.
[41] S. Kanemura, T. Kasai, G.-L. Lin, Y. Okada, J.-J. Tseng, et al., Phenomenology of Higgs bosons in the Zee model, Phys. Rev. D 64 (2001) 053007, arXiv:hep-ph/0011357, InSPIRE.
[42] K. Kannike, Vacuum stability conditions from copositivity criteria, Eur. Phys. J. C 72 (2012) 2093, arXiv:1205.3781, InSPIRE.
[43] G. Degrassi, S. Di Vita, J. Elias-Miro, J.R. Espinosa, G.F. Giudice, et al., Higgs mass and vacuum stability in the Standard Model at NNLO, J. High Energy Phys. 1208 (2012) 098, arXiv:1205.6497, InSPIRE.
[44] ATLAS Collaboration, Measurements of the properties of the Higgs-like boson in the two photon decay channel with the ATLAS detector using 25 fb^{-1} of proton–proton collision data, InSPIRE.
[45] CMS Collaboration, Updated measurements of the Higgs boson at 125 GeV in the two photon decay channel, InSPIRE.
[46] M. Carena, I. Low, C.E. Wagner, Implications of a modified Higgs to diphoton decay width, J. High Energy Phys. 1208 (2012) 060, arXiv:1206.1082, InSPIRE.
[47] J.R. Ellis, M.K. Gaillard, D.V. Nanopoulos, A phenomenological profile of the Higgs boson, Nucl. Phys. B 106 (1976) 292, InSPIRE.
[48] M.A. Shifman, A. Vainshtein, M. Voloshin, V.I. Zakharov, Low-energy theorems for Higgs boson couplings to photons, Sov. J. Nucl. Phys. 30 (1979) 711–716, InSPIRE.
[49] J.F. Gunion, H.E. Haber, G.L. Kane, S. Dawson, The Higgs Hunter's guide, Front. Phys. 80 (2000) 1–448, InSPIRE.
[50] C.-S. Chen, C.-Q. Geng, D. Huang, L.-H. Tsai, New scalar contributions to $h \to Z\gamma$, Phys. Rev. D 87 (2013) 075019, arXiv:1301.4694, InSPIRE.

[51] M. Gonzalez-Garcia, M. Maltoni, J. Salvado, T. Schwetz, Global fit to three neutrino mixing: critical look at present precision, J. High Energy Phys. 1212 (2012) 123, arXiv:1209.3023, InSPIRE.
[52] D. Forero, M. Tortola, J. Valle, Global status of neutrino oscillation parameters after Neutrino-2012, Phys. Rev. D 86 (2012) 073012, arXiv:1205.4018, InSPIRE.
[53] G. Fogli, E. Lisi, A. Marrone, D. Montanino, A. Palazzo, et al., Global analysis of neutrino masses, mixings and phases: entering the era of leptonic CP violation searches, Phys. Rev. D 86 (2012) 013012, arXiv:1205.5254, InSPIRE.
[54] D. Schmidt, T. Schwetz, H. Zhang, Status of the Zee–Babu model for neutrino mass and possible tests at a like-sign linear collider, arXiv:1402.2251, InSPIRE.